Late Cretaceous evolution of the Coqen Basin (Lhasa terrane) and implications for early topographic growth on the Tibetan Plateau

Gaoyuan Sun[1], Xiumian Hu[1†], Hugh D. Sinclair[2], Marcelle K. BouDagher-Fadel[3], and Jiangang Wang[4]

[1]*State Key Laboratory of Mineral Deposits Research, School of Earth Sciences and Engineering, Nanjing University, Xianlin Dadao 163, Nanjing, 210023, China*

[2]*School of GeoSciences, University of Edinburgh, Drummond Street, Edinburgh EH8 9XP, Scotland, UK*

[3]*Department of Earth Sciences, University College London, London WC1H 0BT, UK*

[4]*State Key Laboratory of Lithospheric Evolution, Institute of Geology and Geophysics, Chinese Academy of Sciences, Beijing, 100029, China*

ABSTRACT

The tectonic evolution of the Lhasa terrane (southern Tibetan Plateau) played a fundamental role in the formation of the Tibetan Plateau. However, many uncertainties remain with regard to the tectonic and paleogeographic evolution of the Lhasa terrane prior to the India-Asia collision. To determine the early tectonic processes that controlled the topographic evolution of the Lhasa terrane, we analyze the Cretaceous strata exposed in the Coqen Basin (northern Lhasa subterrane), which comprises the Langshan and Daxiong Formations. The Langshan Formation unconformably overlies the volcanic rocks of the Lower Cretaceous Zelong Group and consists of ~80 m of *Orbitolina*-bearing limestones, which were deposited in a low-energy, shallow marine environment. Micropaleontological analysis indicates that the Langshan Formation in the Coqen Basin was deposited from late Aptian to early Cenomanian times (ca. 113–96 Ma). The overlying Daxiong Formation (~1700 m thick) consists of conglomerate, coarse sandstone, and siltstone with interbedded mudstone, and represents deposits of alluvial fans and braided rivers. The Daxiong Formation was deposited after the early Cenomanian (ca. 96 Ma) and accumulated until at least ca. 91 Ma, indicating accumulation rates of greater than 0.3 km m.y.$^{-1}$. By combining paleocurrent data, sandstone petrology, detrital zircon U-Pb ages, and Hf isotope analysis, we demonstrate that the Daxiong Formation was derived from Lower Cretaceous volcanic rocks and pre-Cretaceous strata in the northern Lhasa subterrane. During Late Cretaceous time, two thrust systems with opposite vergence were responsible for transforming the northern Lhasa subterrane into an elevated mountain range. This process resulted in the evolution from a shallow marine environment (Langshan Formation) into a terrestrial depositional environment (Daxiong Formation) on the southern margin of the northern Lhasa subterrane. Given the regional paleogeographic context, we conclude that the Daxiong Formation in the Coqen Basin records local crustal shortening and flexure resulting in foreland basin development on the southern margin of the northern Lhasa subterrane, which implies early topographic growth of the northern Lhasa subterrane in southern Tibet prior to the India-Asia collision.

INTRODUCTION

The Tibetan Plateau has an average elevation of >5000 m and comprises the Lhasa, Qiangtang, Songpan-Ganzi, and Kunlun terranes from south to north (Fig. 1A). The formation of the Tibetan Plateau has exerted substantial control over the Asian climate, monsoon intensity, and ocean chemistry (Raymo and Ruddiman, 1992; Richter et al., 1992; An et al., 2001). However, the timing of the initial topographic uplift of the Tibetan Plateau remains an important question, and significant uncertainty remains (Tapponnier et al., 2001; Rowley and Currie, 2006; Wang et al. 2008; Najman et al., 2010; Dai et al., 2012, 2013; Ding et al., 2014; Staisch et al., 2014). Recently, oxygen isotope–based paleoaltimetry studies in the northern Lhasa subterrane and Qiangtang terrane have revealed that the central Tibetan Plateau may have reached elevations greater than 4000 m, forming the present arid environment, by late Oligocene time (e.g., ca. 28–26 Ma; DeCelles et al., 2007a; Xu et al., 2013).

Low-temperature thermochronology reveals that central Tibet experienced rapid to moderate exhumation in the Late Cretaceous (ca. 85–70 Ma), which was followed by slow erosional exhumation during the Eocene (ca. 55–45 Ma; Hetzel et al., 2011; Rohrmann et al., 2012). Structural restorations imply substantial crustal shortening throughout the Cretaceous (Pan, 1993; Murphy et al., 1997; Kapp et al., 2005, 2007a; Volkmer et al., 2007). Clearly, paleoaltimetry, rock exhumation, and crustal shortening record different processes, but these processes are all related to the topographic growth of the Tibetan Plateau. The contrasts in timing imply certain uncertainties in the spatial and temporal growth of Tibet. We address this problem by further examining sedimentological evidence from the northern Lhasa subterrane regarding relative uplift and erosion, and place this evidence within the context of the early tectonic history of the southern Tibetan region.

Cretaceous sedimentary basins in the Lhasa terrane can be divided into two domains separated by the Gangdese magmatic arc. To the south of the Gangdese arc, the Xigaze forearc basin comprises thick marine turbidites, which were derived mostly from the Gangdese magmatic arc (Dürr, 1996; Wu et al., 2010; Wang et al., 2012; An et al., 2014; Orme et al., 2014). To the north of the Gangdese arc (the northern Lhasa subterrane), there are widespread Cretaceous sedimentary basins, such as the Linzhou Basin, Nima Basin, Selin Co Basin, and Coqen Basin (Fig. 1B; Leier et al., 2007a; DeCelles et al., 2007b; Kapp et al., 2007a; Zhang et al., 2011; this study). Throughout the Cretaceous, the Lhasa terrane was influenced by the subduction of the Neotethyan oceanic lithosphere along its southern border and collision with the

†E-mail: huxm@nju.edu.cn

GSA Bulletin; July/August 2015; v. 127; no. 7/8; p. 1001–1020; doi: 10.1130/B31137.1; 14 figures; 1 table; Data Repository item 2015082; published online 19 February 2015.

For permission to copy, contact editing@geosociety.org
© 2015 Geological Society of America

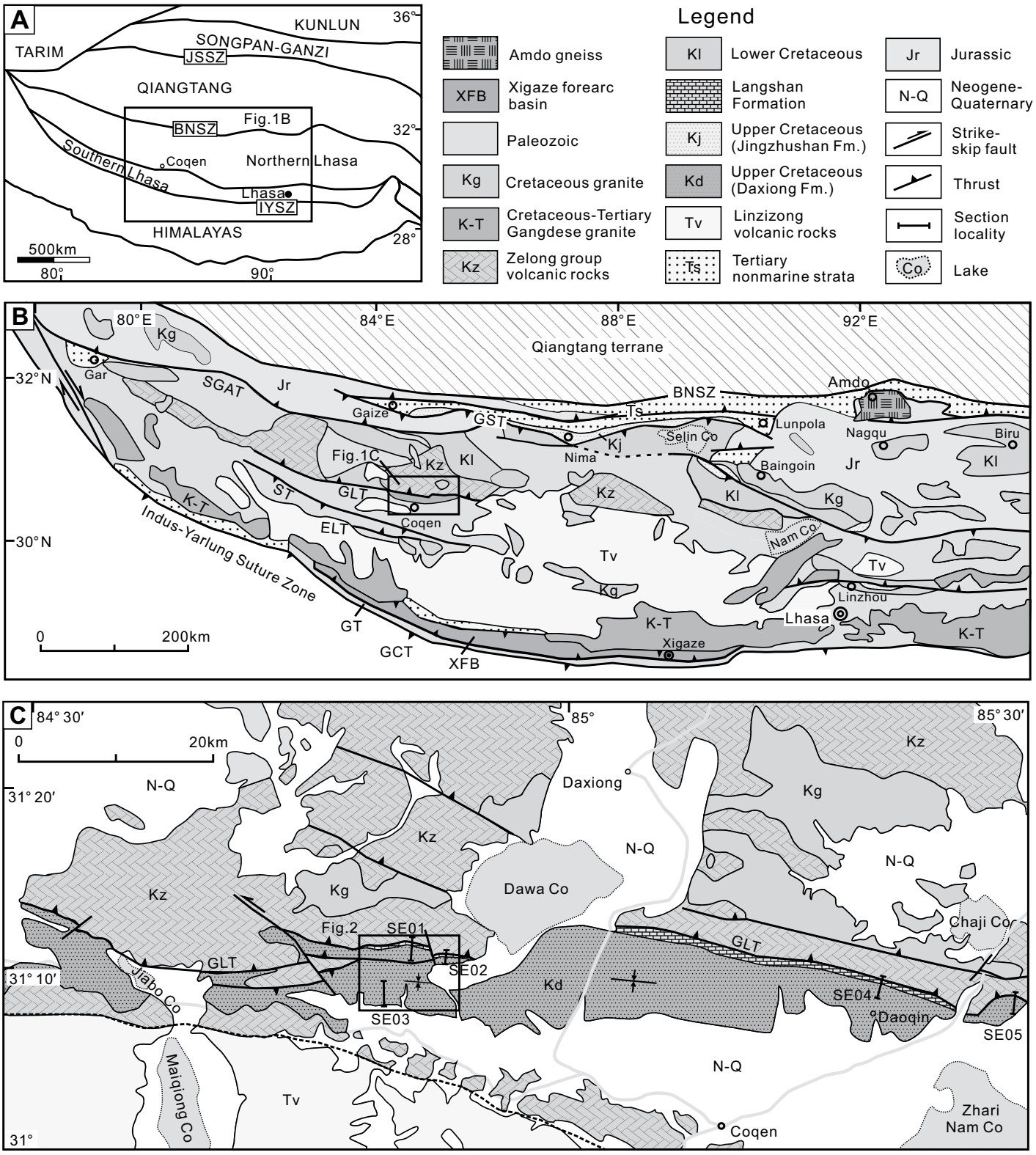

Figure 1. (A) Simplified tectonic map of the Tibetan Plateau and adjacent regions, showing the Lhasa terrane in the context of the Tibetan Plateau (Pan et al., 2004). JSSZ—Jinsha suture zone; BNSZ—Bangong-Nujiang suture zone; IYSZ—Indus-Yarlung suture zone. (B) Simplified geological map of the Lhasa terrane modified from Kapp et al. (2005). SGAT—Shiquan-Gaize-Amdo thrust; GST—Gaize–Selin Co thrust; GLT—Gugu La thrust; ST—Shibaluo thrust; ELT—Emei La thrust; GT—Gangdese thrust system; GCT—Great Counter thrust. (C) Simplified geological map of the Coqen Basin, showing the studied sections (SE01–SE05) in the north of Coqen County, modified from the 1:250,000-scale regional geological survey in Tibet (Coqen area) (Liu et al., 2004).

Qiangtang terrane along its northern flank. During late Aptian to Cenomanian times, the northern Lhasa subterrane was close to sea level, and shallow marine sediments accumulated (Zhang, 2000; Zhang et al., 2004, 2012; Leier et al., 2007b). Subsequently, widespread continental sedimentation prevailed on the northern Lhasa subterrane (Leier et al., 2007a; DeCelles et al., 2007b; Zhang et al., 2011, 2012). The tectonic type of these basins is still debated due to the limited analysis of the stratigraphy, sedimentology, and provenance of the Cretaceous strata. The Coqen Basin, located in the interior of the Lhasa terrane (southern Tibetan Plateau; Fig. 1C), provides a well-exposed succession of Cretaceous strata that enables the above models of basin formation to be further tested, thereby improving our understanding of the topographic controls at the time the basin formed.

To evaluate the origins of the Late Cretaceous Coqen Basin, this study initially constrains the timing of deposition of the Langshan and Daxiong Formations through micropaleontology and U-Pb dating of a key tuff horizon. We then characterize the depositional history of the Upper Cretaceous strata through sedimentology and through provenance data including sandstone petrology, paleocurrents, detrital zircon U-Pb ages, and Hf isotope analysis on the Daxiong Formation. There are numerous published zircon U-Pb ages and Hf isotope data from the Tibetan Plateau that record distinctive signals from the different tectonic regions, and this body of work permits sediment source regions to be reconstructed (Leier et al., 2007c; Zhu et al., 2009, 2011a; Gehrels et al., 2011, and references therein). The stratigraphic evolution of the basin is then compared to other coeval basins in the Lhasa terrane. Based on the provenance, sedimentology, and regional context, we suggest that the Late Cretaceous Coqen Basin is likely to have recorded foreland basin accumulation in which the flexure subsidence was controlled by thrust loading in the northern Lhasa subterrane.

GEOLOGIC BACKGROUND

Regional Tectonic Units

The Lhasa terrane is located on the southern Tibetan Plateau (Fig. 1B) and represents the last terrane accreted onto southern Asia before the India-Asia collision (Allégre et al., 1984; Dewey et al., 1988; Yin and Harrison, 2000). North of the Lhasa terrane, the Bangong-Nujiang suture zone separates the Lhasa and Qiangtang terranes (Fig. 1B) and represents the remains of the Bangong-Nujiang Ocean that closed during the Late Jurassic–Early Cretaceous (Allégre et al., 1984; Dewey et al., 1988; Yin and Harrison, 2000; Kapp et al., 2005). The Bangong-Nujiang suture zone continues for at least 1200 km east-west along strike and is dominated by Jurassic deep-water turbidites, mélanges, and ophiolite fragments (Yin and Harrison, 2000; Kapp et al., 2005). There are also Cretaceous to Cenozoic fluvial sandstones and conglomerates with interbedded volcanic rocks documented in the suture zone (e.g., northern Nima Basin; Kapp et al., 2007a; DeCelles et al., 2007b). North of the Bangong-Nujiang suture zone, upper Paleozoic shallow marine deposits and Lower Jurassic blueschist-bearing mélanges are widely distributed in the central metamorphic belt of the Qiangtang terrane (Cheng and Xu, 1986; Liu, 1988; Kapp et al., 2000, 2003a). Only a few Cretaceous strata are present in the west and central part (Cheng and Xu, 1987; Kapp et al., 2005) with limited exposures of Cenozoic nonmarine rocks trending east-west (Cheng and Xu, 1987; Kapp et al., 2005).

To the south of the Lhasa terrane, the Indus-Yarlung suture zone separates the Lhasa terrane from the Tethys Himalaya and represents the remnants of the subducted Neotethyan oceanic plate (Fig. 1A) (Yin and Harrison, 2000). The timing of the India-Asia collision is middle to late Paleocene, as documented by the first arrival of Asia-derived siliciclastic sediments on the northern Tethyan shelf and by the recognition of the foreland forebulge (e.g., Wang et al., 2011; Hu et al., 2012; DeCelles et al., 2014; Wu et al., 2014).

The Lhasa terrane comprises two tectonic domains: the southern Lhasa subterrane (Gangdese magmatic arc and Xigaze forearc basin) and the northern Lhasa subterrane (Burg et al., 1983; England and Searle, 1986; Searle et al., 1987). The Gangdese magmatic arc is characterized by the Late Triassic–early Cenozoic Gangdese batholiths and Cenozoic Linzizong volcanic rocks (Chu et al., 2006; Mo et al., 2007, 2008; Wen et al., 2008; Ji et al., 2009; Lee et al., 2009; Zhu et al., 2011a), which were formed by northward subduction of Neotethyan oceanic lithosphere beneath the Lhasa terrane (Yin and Harrison, 2000; Ding et al., 2003; Ji et al., 2009). Thick sequences of Albian–Campanian deep-water turbidites were deposited in the Xigaze forearc basin, which was located on the southern margin of the Gangdese magmatic arc (Dürr, 1996; Wang and Liu, 1999; Wang et al., 2012). Provenance analysis reveals that the southern Lhasa subterrane (Gangdese magmatic arc) represented the main source for the Xigaze forearc basin (Wu et al., 2010; An et al., 2014; Orme et al., 2014). Cretaceous magmatic rocks are also widespread in the northern Lhasa subterrane (e.g., Lower Cretaceous Zelong Group volcanic rocks; Zhu et al., 2006, 2009). Pre-Cretaceous strata exposed in the northern Lhasa subterrane are represented by Carboniferous metasedimentary rocks, Permian limestone, and Jurassic siliciclastic successions (Leeder et al., 1988; Yin et al., 1988). There is also more than 4 km of Cretaceous strata preserved in the northern Lhasa subterrane, with Lower Cretaceous strata present in many places, such as the Linzhou, Selin Co, and Coqen Basins, which contain marginal marine and deltaic clastic sedimentary rocks interbedded with volcanic tuffs (Zhang et al., 2004; He et al., 2007; Leier et al., 2007a, 2007b; Volkmer et al., 2007; Zhang et al., 2012), and the southern Nima Basin, which contains alluvial conglomerates (Kapp et al., 2007a; DeCelles et al., 2007b). The late Aptian to early Cenomanian *Orbitolina*-bearing Langshan Formation limestone is extensively exposed in the northern Lhasa subterrane (XZBGM, 1993; Zhang, 2000; Scott et al., 2010). The Upper Cretaceous strata record continental deposition and comprise the Daxiong Formation in the Coqen Basin (this study), the Takena Formation in the Linzhou Basin (Leier et al., 2007a), and the Jingzhushan Formation in the southern Nima and Selin Co Basins (Kapp et al., 2007a; DeCelles et al., 2007b; Zhang et al., 2012).

Geology of the Study Area

The study area is located between Coqen County and Dawa Co (lake) on the northern Lhasa subterrane and broadly comprises Cretaceous igneous and sedimentary rocks (Fig. 1C) (Liu et al., 2004; Zhang et al., 2004; Zhu et al., 2006). The Lower Cretaceous Zelong Group volcanic rocks, with a thickness of at least 1000 m, are widely exposed. These rocks are composed mainly of intermediate to felsic lavas with minor mafic rocks. Together with coeval intrusive granites, these rocks represent a magmatic arc in the northern Lhasa subterrane (Zhu et al., 2006, 2009, 2011a; Zhou et al., 2008). Recent zircon U-Pb studies reveal that the ages of Zelong Group volcanic rocks are between 143 and 102 Ma, with a magmatic flare-up at ca. 110 Ma (Zhu et al., 2008, 2009, 2011a).

Overlying the volcanic rocks of the Zelong Group, the Langshan Formation is a limestone unit characterized by abundant benthic foraminifera and bivalves (XZBGM, 1993; Scott et al., 2010). The Daxiong Formation (referred to as the Upper Cretaceous conglomerate unit by Murphy et al. [1997], and the Jingzhushan Formation by XZBGM [1993], Liu et al. [2004], and Pan et al. [2004]) unconformably overlies the Langshan Formation and comprises thick conglomerate and sandstone beds with interbedded volcanic tuffs. This formation is exposed

along an east-west belt that is ~100 km long and 10 km wide (Fig. 1C). In the Coqen Basin, the Daxiong Formation is deformed into an east-west–trending syncline cross-cut by faults (Fig. 2). The Cenozoic Linzizong volcanic rocks unconformably overlie the deformed Daxiong Formation in the Coqen Basin (Liu et al., 2004).

Structural Setting

Structural analyses and regional mapping of the Lhasa terrane demonstrate that substantial upper crustal deformation and shortening predated the India-Asia collision, with ~290 km of Cretaceous shortening over the modern north-south distance of ~310 km (Pan, 1993; Murphy et al., 1997; Kapp et al., 2005, 2007a, 2007b; Volkmer et al., 2007; Pullen et al., 2008). In the study area, the main structures are parts of the "Northern Lhasa thrust belt" of Murphy et al. (1997), which include the Gugu La, Shibaluo, and Emei La thrusts (Fig. 1B). The Langshan Formation limestone was incorporated into this thin-skinned thrust belt, whereas the gently dipping Cenozoic Linzizong volcanic tuffs locally overlie this thrust belt. These relationships reveal that crustal shortening and deformation occurred during the Cretaceous. Furthermore, the deformation documented in the Xiagangjiang region (~30 km north of the study area) revealed ~103 km of shortening (~53%) via the south-directed thrust system during Late Cretaceous to Paleocene times (Volkmer et al., 2007). Collectively, the Late Cretaceous deformation in the northern Lhasa subterrane is characterized by oppositely vergent thrust belts: the north-dipping Gugu La thrust and south-dipping Gaize–Selin Co thrust (Fig. 1B; Murphy et al., 1997; Kapp et al., 2007a). The Gugu La thrust placed the Lower Cretaceous Zelong volcanic rocks over the Upper Cretaceous Daxiong Formation and included south-vergent fault-bend folds in the hanging wall of the thrust. These structures are cross-cut by granitoid intrusions dated to ca. 92–80 Ma (Murphy et al., 1997); hence, the deformation must have taken place prior to this age. The Gaize–Selin Co thrust initiated after ca. 99–97 Ma, based on the syn-depositional strata, and placed the Langshan Formation in the hanging wall against the Upper Cretaceous Jingzhushan Formation in the footwall (Kapp et al., 2007a).

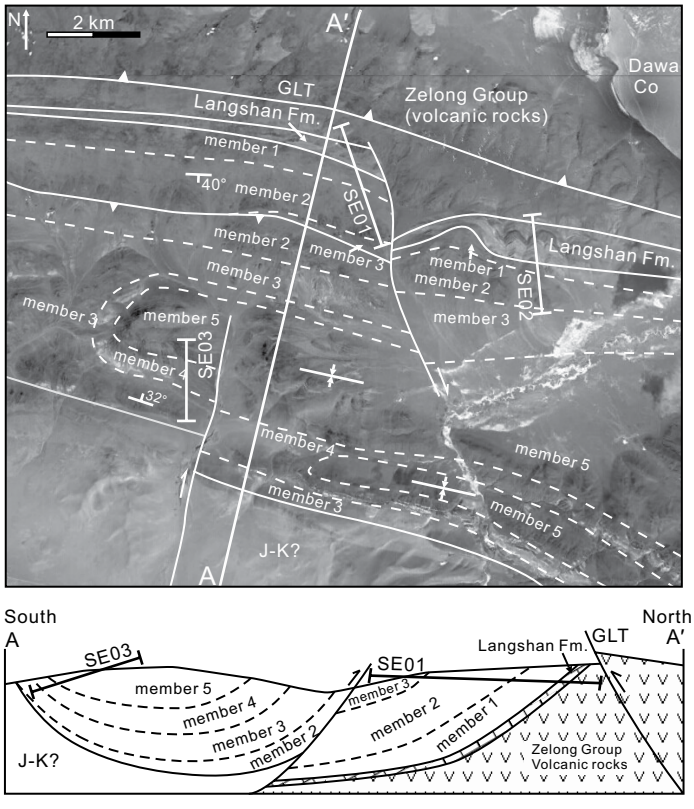

Figure 2. Satellite image of the studied sections from Google Earth. The location of the cross-section is shown in the satellite image. Members 1–5 are of the Daxiong Formation. SE01–SE03 are studied sections. GLT—Gugu La thrust; J-K?—Jurassic–Cretaceous(?) rocks.

METHODS

Sedimentology and Paleocurrent Data

We measured stratigraphic sections in detail at five locations (Fig. 1C). Through the investigation of lithofacies associations and sedimentary features, the probable depositional environments and sedimentary mircofacies were distinguished. The lithofacies analysis followed the methods of Miall (1978, 1996) and DeCelles et al. (1991). The paleocurrent data were measured in the field from cross-stratification and clast imbrication in sandstone and conglomerate beds. All original measured data were corrected to horizontal using standard stereonet techniques, and the average trough-axis orientation of each point was measured and determined statistically on a stereographic plot of 15–20 trough limbs (method I of DeCelles et al., 1983).

Conglomerate and Sandstone Provenance Analysis

The conglomerate compositions were quantified by counting clast types at 10 locations in the field using a 10 cm grid and at least 100 clasts per site. A total of 36 standard petrographic thin sections were point-counted according to the Gazzi-Dickinson method (Ingersoll et al., 1984). Approximately 400 grains were counted per site, and the data were normalized for plotting on standard ternary diagrams.

Detrital Zircon U-Pb Dating and Hf Isotopes

Detrital zircons were separated from the medium-grained sandstones of the Daxiong Formation. U-Pb dating was conducted at the State Key Laboratory for Mineral Deposits Research, Nanjing University, China. The U-Pb ages were obtained via laser ablation inductively coupled plasma mass spectrometry (LA-ICP-MS) following the method described by Jackson et al. (2004). The ages described in this study are $^{206}Pb/^{238}U$ ages for grains with ages younger than 1000 Ma and $^{207}Pb/^{206}Pb$ ages for grains older than 1000 Ma. The results presented in this study exclude analyses with >20% discordance. Further details of the instrumental conditions and data acquisition are published in He et al. (2010). The age results were calculated using GLITTER software (version 4.4) (Van Achterbergh et al., 2001), and common Pb corrections were conducted following Andersen (2002). Weighted average age calculations, determination of detrital zircon age probabilities, and plotting of concordia diagrams were performed using Isoplot software (version 2.49)

(Ludwig, 2001). The uncertainties in the single grain and weighted average ages, including all known analytical and systematic errors, are cited at the 1σ and 2σ levels, respectively.

Hf isotope analysis was performed on the detrital zircon grains with U-Pb ages and was conducted at the State Key Laboratory for Mineral Deposits Research, Nanjing University, China. The zircon Hf isotopic compositions were obtained via a Thermo Scientific Neptune Plus mass spectrometer Multicollector-ICP-MS coupled to a New Wave UP193 solid-state laser ablation system. Zircons were ablated with a beam diameter of 35 μm and a laser repetition rate of 8 Hz. The results for every zircon were collected 200 times in one minute. For the calculation of the results, we applied 1.865×10^{-11} a^{-1} for the decay constant of ^{176}Lu (Scherer et al., 2001). The calculation of $\varepsilon_{Hf}(t)$ and Hf model age (T^{C}_{DM}) followed the methodologies of Bouvier et al. (2008) and Griffin et al. (2002), respectively.

The youngest detrital zircon ages can commonly be applied to constrain the maximum depositional ages of stratigraphic units (Dickinson and Gehrels, 2009). The comparison of age compilations between the detrital and the igneous zircons of potential source areas can reveal remarkably similar age spectra. In addition, the zircon Hf isotopic compositions characterize distinctive crustal histories, which also yield important information on the sedimentary provenance and tectonic setting of the basin in which the zircons accumulated (Wu et al., 2010; Cawood et al., 2012).

STRATIGRAPHY AND SEDIMENTOLOGY

In the study area, the strata from the bottom to the top consist of the Zelong Group volcanic rocks, the Langshan Formation, and the Daxiong Formation (Figs. 3 and 4).

Langshan Formation

In sections SE01 and SE02, the Langshan Formation unconformably overlies the Zelong volcanic rocks; in sections SE04 and SE05, the same boundary is marked by a fault (Murphy et al., 1997; Liu et al., 2004). A hardground surface is observed at the top of the Langshan Formation (Fig. 5C), and this surface separates the Langshan Formation from the overlying Daxiong Formation. The average thickness of the Langshan Formation in our measured sections is ~80 m. The lithofacies associations in the Langshan Formation are dominated by wackestones and packstones that consist of abundant benthic foraminifera throughout the entire section (Fig. 6A). For example, the lower part contains *Ammobaculites* sp., *Vercorsella arenata*, *Cuneolina parva*, *Cuneolina pavonia*, *Mesorbitolina* cf. *texana*, *Pseudocyclammina* cf. *rugosa*, and *Nezzazata* sp., and the upper part contains *Orbitolina qatarica*, *Conicorbitolina concava*, and *Conicorbitolina conica* (Appendix Plate S1 [GSA Data Repository][1]). There are several thin, interbedded marly siltstone and wackestone in section SE01. Based on these foraminiferal assemblages and lithofacies associations, we interpret the Langshan Formation to have been deposited in a low-energy lagoonal and shallow reefal environment (BouDagher-Fadel, 2008, 2013).

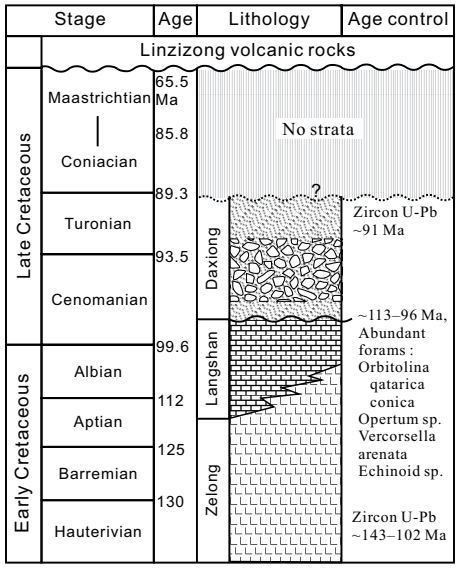

Figure 3. Generalized Cretaceous stratigraphy of the Coqen Basin. Lithological assemblages and ages are based on XZBGM (1993), Zhu et al. (2009), Scott et al. (2010), and this study. See Figure 4 for lithologic symbols.

Daxiong Formation

Synthesizing information from the field outcrops and lithofacies assemblages from the studied region, we identified five informal members of the Daxiong Formation that record variations in the dominant lithofacies (Fig. 4). A simple accumulation rate calculation indicates that the Daxiong Formation was deposited at a rate of more than 0.3 km m.y.$^{-1}$, based on the total thickness (compacted thickness of ~1.7 km) and depositional interval (ca. 96–91 Ma). A total of nine sedimentary lithofacies were identified in the Daxiong Formation (Table 1).

Member 1

Description. Member 1 is nearly 220 m thick in sections SE01 and SE05 and at least 100 m thick in sections SE02 and SE04. This member is composed mainly of red, medium- and coarse-grained volcaniclastic sandstone beds, which extend laterally for tens of meters and generally feature lenticular geometries. Upward-fining packages are commonly 1.5–1.8 m thick and are separated from one another by abrupt erosion surfaces along their bases. Individual sandstone packages tend to have thin conglomeratic or very coarse-grained sandstone beds (~10–50 cm; lithofacies G1). These beds feature abundant siltstone and/or mudstone intraclasts in their lowest portions and commonly exhibit slight normal grading near their bases. The contact between the lowest parts of these beds and the underlying siltstone is sharp. In the middle part of a package, the medium- and coarse-grained sandstone beds exhibit abundant low-angle planar cross-bedding of ~20–50 cm thickness (Fig. 5D; lithofacies S1). These beds alternate with fine- to medium-grained sandstones with medium- to small-scale (commonly decimeter-scale) high-angle trough and planar cross-stratification and current ripple laminations (Fig. 5E; lithofacies S2 and S3). The uppermost parts of a package comprise thin (~10–20 cm), fine-grained, horizontally and ripple-laminated siltstone or mudstone beds (lithofacies F1). Overall, the grains of these sandstones are relatively uniform and are dominated by the coarse grain size. The paleocurrent data from the trough cross-stratification in this member reveal a southward paleoflow direction (Fig. 7).

Interpretation. Based on the characteristics of the fining-upward sandstone packages (commonly 1.5–1.8 m thick), we interpret the lithofacies associations of member 1 as having been deposited by shallow (<2 m of water depth), laterally unstable, sandy braided rivers (Miall, 1978; Lunt and Bridge, 2004; Bridge and Lunt, 2006). The low-angle cross-bedding records the migration of braided bar forms. The high-angle trough and planar cross-stratification was deposited by the migration of subaqueous three-dimensional and two-dimensional dunes within the paleochannels, respectively. The horizontally laminated sandstones are interpreted as having been deposited under upper-stage unidirectional flow conditions within infilled channels or bar tops (i.e., very shallow depths). The siltstone beds on top of the upward-fining packages represent deposition in abandoned channels during the waning stages of flow (Bristow, 1993).

[1]GSA Data Repository item 2015082, Supplementary foraminiferal plate, detrital model compositions, and zircon data, is available at http://www.geosociety.org/pubs/ft2015.htm or by request to editing@geosociety.org.

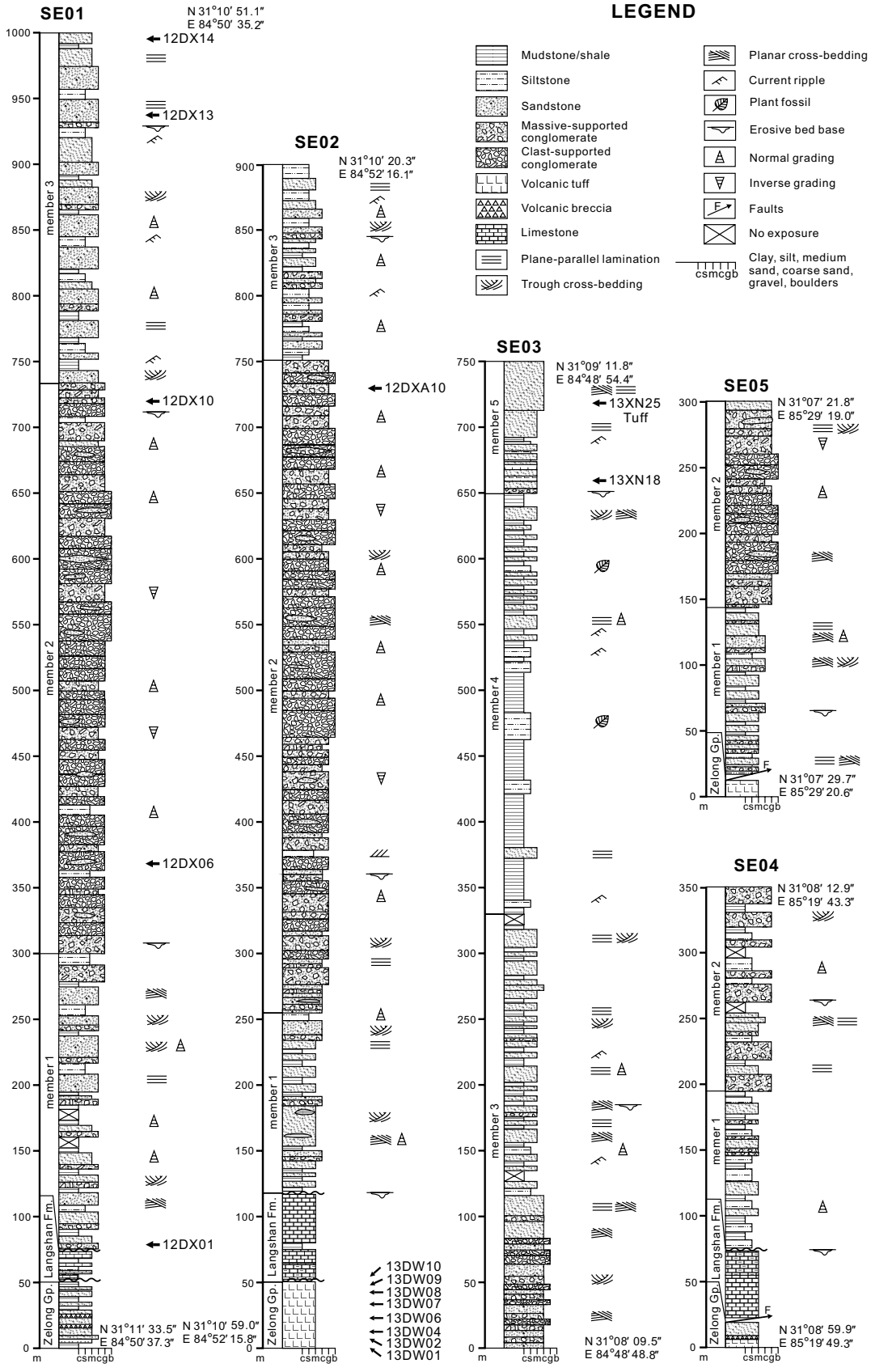

Figure 4. Lithological columns and sedimentary symbols of the measured sections SE01–SE05; sample locations for zircon analyses are indicated by arrows.

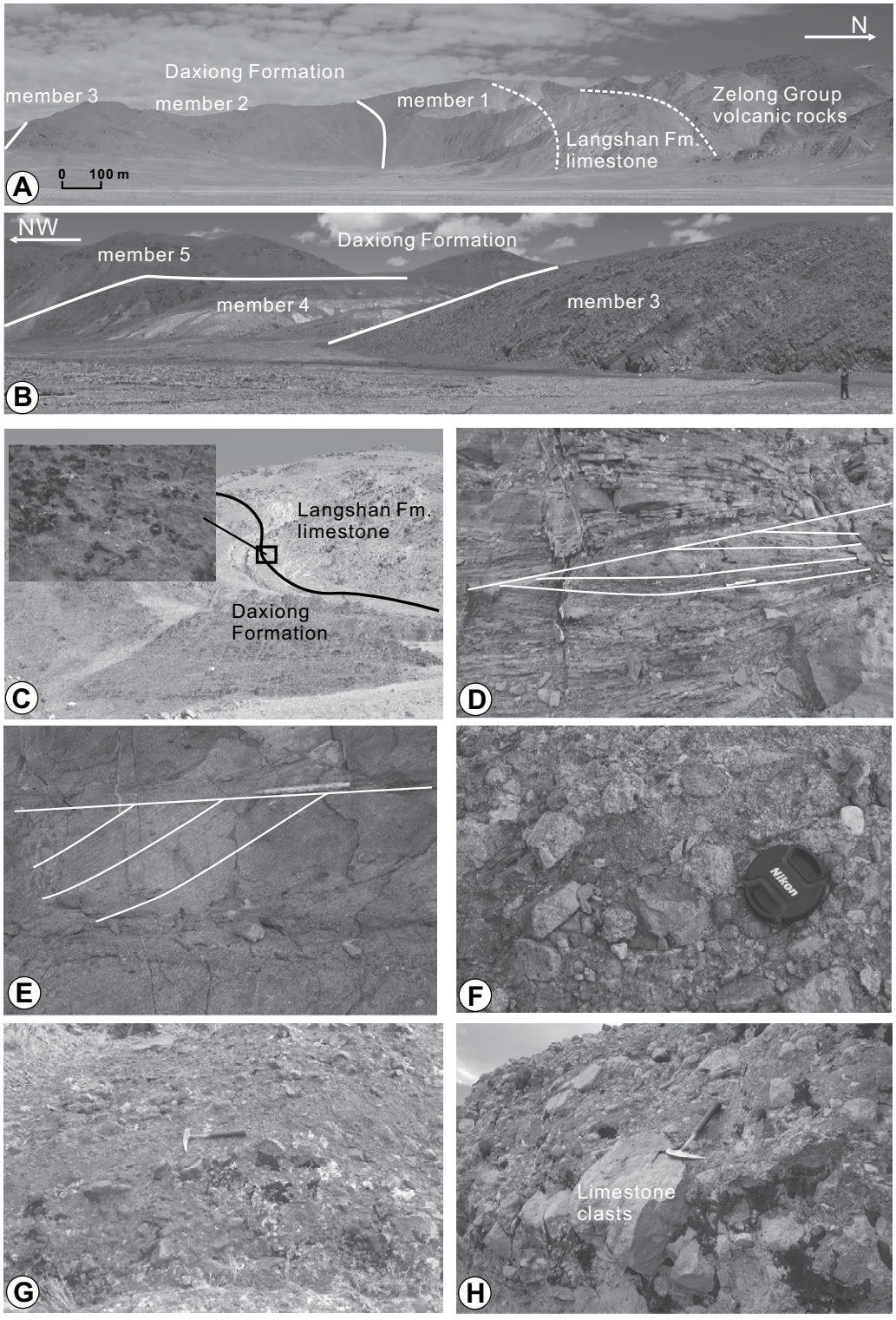

Figure 5. (A) Panoramic photograph for section SE01, showing the lower parts of the Daxiong Formation and the relationship with the underlying strata. (B) Panoramic photograph for section SE03, showing the upper part of the Daxiong Formation. (C) Unconformable contact between the Langshan Formation and the Daxiong Formation. The inset photo is of a bedding plane of the hardground on the top of the Langshan Formation, showing a depositional hiatus. (D) Coarse sandstone beds with low-angle (<20°) planar cross-stratification (section SE01, member 1). Pen is 17 cm long. (E) Medium-coarse sandstone beds with high-angle (>20°) trough cross-stratification (section SE05, member 1). Pen is 15 cm long. (F) Abundant volcanic clasts in the Daxiong Formation (section SE01, member 2). (G) Clast-supported cobble conglomerate beds with imbricated clasts (section SE02, member 2). Hammer is 41 cm long; (H) Massive matrix-supported conglomerate beds, abundant in limestone clasts (section SE05, member 2). Hammer is 41 cm long.

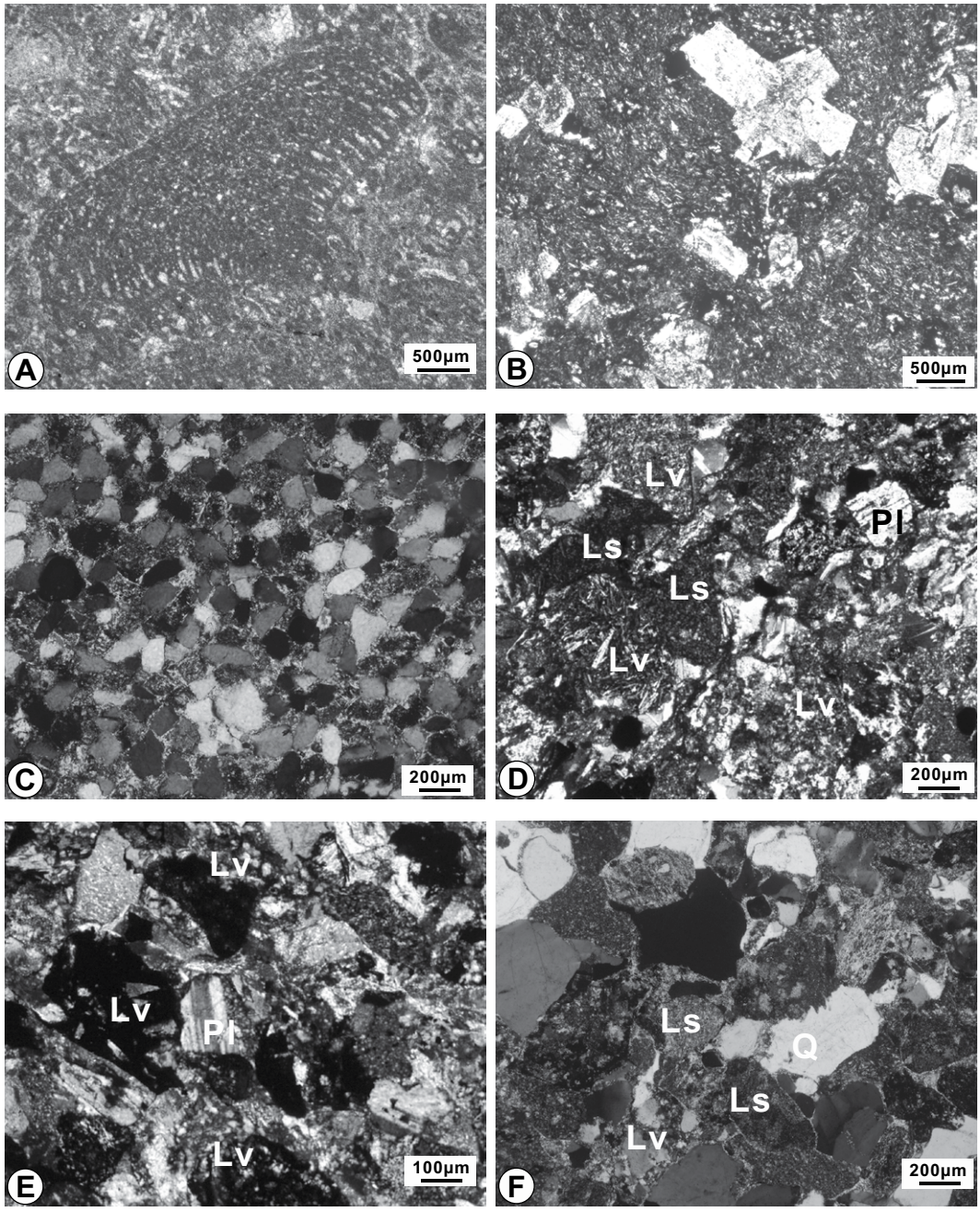

Figure 6. Petrography of the Langshan and Daxiong Formations. (A) *Orbitolina*-bearing limestone from the Langshan Formation (sampled at 30 m, section SE02). (B) Andesite pebble (400 m, member 2 of the Daxiong Formation, section SE02). (C) Quartz-rich sandstone pebble (405 m, member 2, section SE02). (D) Lithic sandstone (250 m, member 1, section SE01), showing abundant volcanic fragments. (E) Lithic sandstone (990 m, member 3, section SE01), showing volcanic and sedimentary fragments. (F) Lithic sandstone (720 m, member 5, section SE03), in which lithic fragments are mostly sedimentary rocks. Q—quartz; Pl—plagioclase; Lv—volcanic rock fragment; Ls—sedimentary fragment.

Member 2

Description. Member 2 is well exposed in the study area and has an average thickness of at least 500 m. The lithofacies of this member consist of many fining-upward sequences of red and gray conglomerate beds with thicknesses of 3–5 m and minor wedges and lenses of coarse sandstone and siltstone interbeds (~20–50 cm in thickness). The clasts are predominantly angular to subrounded and poorly sorted. Their compositions are mainly volcanic with minor limestone, mudstone, and quartz-rich sandstone clasts (Fig. 5F). However, in section SE05, limestone clasts represent nearly 15% of the total clasts. The clast- and matrix-supported conglomerate lithofacies are abundant in the conglomerate beds of this member.

The clast-supported conglomerate beds are composed of pebble- to cobble-sized clasts that are poorly to moderately sorted, and commonly exhibit crude horizontal stratification with imbricated clasts (Fig. 5G). Erosional basal surfaces are common and abruptly overlie the underlying siltstone beds. The average clast size is ~15 cm in the long dimension, with a maximum clast size of ~30 cm (lithofacies G2). The massive matrix-supported conglomerate beds (commonly ~5 m in thickness) have disorganized pebble- to boulder-sized clasts (Fig. 5H), all of which are poorly sorted and contained within a muddy or sandy matrix. The clasts are angular, and larger clasts are located at the top of the bed, generating inverse grading. Several of these beds have a maximum clast size greater than 50 cm (lithofacies G3).

Lenticular or wedge-shaped beds of (very) coarse-grained sandstone are locally intercalated within the discontinuous conglomerate beds. These sandstones typically exhibit

TABLE 1. LITHOFACIES FOUND IN THE MEASURED SECTIONS (THE DAXIONG FORMATION), COQEN BASIN, TIBETAN PLATEAU, AND THE INTERPRETATIONS OF THESE LITHOFACIES IN THIS STUDY

Facies code	Description	Process interpretation
G1	Pebble to cobble conglomerate, well sorted and clast supported, subangular to subrounded, slight normal grading, trough cross-stratified and basal erosive boundary. Beds 0.3–1 m thick.	Deposition by bedload on gravelly low-relief bars.
G2	Pebble to very coarse cobble conglomerate, clast supported with a sandy matrix, subrounded gravel, poorly to moderately sorted, crude horizontal bedding, weak grading with imbricated clasts, poorly to moderately organized with few thick layers and basal erosive boundary. Beds 0.5–5 m thick.	Deposition by bedload transport beneath sustained high-velocity, high-sediment-concentration flows.
G3	Medium pebble to medium boulder conglomerate, poorly to moderately sorted, angular to subrounded gravel, clasts randomly oriented, massive conglomerate with a mud-rich matrix-supported fabric, disorganized and unstratified, normal grading or inverse grading. Beds 0.5–5 m thick.	Deposition by matrix-rich debris flows.
S1	Medium- to very coarse-grained sandstone beds with relatively low-angle (<20°) planar cross-stratification and erosional basal surfaces. Beds 0.2–1 m thick.	Deposition by migration of bar bedforms under unidirectional flow.
S2	Medium- to very coarse-grained sandstone with wedge-shaped beds, poorly to moderately sorted, high-angle (>20°) trough cross- and planar stratifications with sandy layers, can be pebbly. Beds 0.2–1.5 m thick.	Deposition by migration of subaqueous large three-dimensional and two-dimensional sandy dunes under unidirectional flow.
S3	Fine- to medium-grained and moderately sorted sandstone with small and asymmetric current ripples. Beds 0.1–1 m thick.	Deposition during migration of ripples under unidirectional flow.
S4	Massive fine- to coarse-grained sandstone, moderately to well sorted, parallel laminated, thin bedded, can be pebbly. Beds 0.2–1 m thick.	Deposition under plane bed and unidirectional flow conditions.
F1	Red mudstone and fine-grained siltstone beds, small current rippled and horizontally laminated, rare carbonate nodules. Beds thickness varies from 0.1 to 2 m.	Deposition in the waning stages of flow or in abandoned channels.
F2	Massive to laminated red, green, or gray siltstone beds bounded at the top by erosive surfaces, horizontally laminated, lens- or wedge-shaped interbedded siltstone and fine-grained sandstone, rare carbonate nodules. Bed thickness is commonly greater than 2 m.	Deposition by suspension fallout from floods on flood plains or distal alluvial plains with high rates of sediment accumulation and intermittent drying, leading to the precipitation of nodules.

Note: Modified after Miall (1978, 1996) and DeCelles et al. (1991).

medium-scale (~0.5 m) planar and trough cross-stratification and planar horizontal lamination (lithofacies S2 and S4). Thin-bedded red siltstones or mudstones are locally present in the uppermost portion of fining-upward packages (lithofacies F1) and are in abrupt contact with the overlying conglomerate beds. The imbricated clasts and interbedded sandstone cross-sets indicate an approximately south-directed flow (Fig. 7).

Interpretation. The lithofacies associations of this middle conglomerate member are interpreted as a record of deposition in an alluvial fan setting (Blair and McPherson, 1994). The clast-supported coarse pebble conglomerate lithofacies (lithofacies G2) with imbricated clasts is interpreted as formed of deposits generated by stream-dominated flows with high sediment concentrations, perhaps during flash floods. The massive, disorganized, matrix-supported and angular to subrounded pebble conglomerate with poor sorting and inverse grading (lithofacies G3) is consistent with debris flows deposited in proximity to medial fans (Naylor, 1980; Blair and McPherson, 1994). The interbedded lenticular or wedge-shaped sandstone and siltstone (lithofacies S2 and S4) at the upper part of the fining-upward sequence are interpreted as the results of deposition during waning flow following ephemeral floods. Certain fine-grained siltstones or mudstones (lithofacies F1) may represent the fine drapes following the high-sediment-concentration flows in a proximal alluvial fan setting.

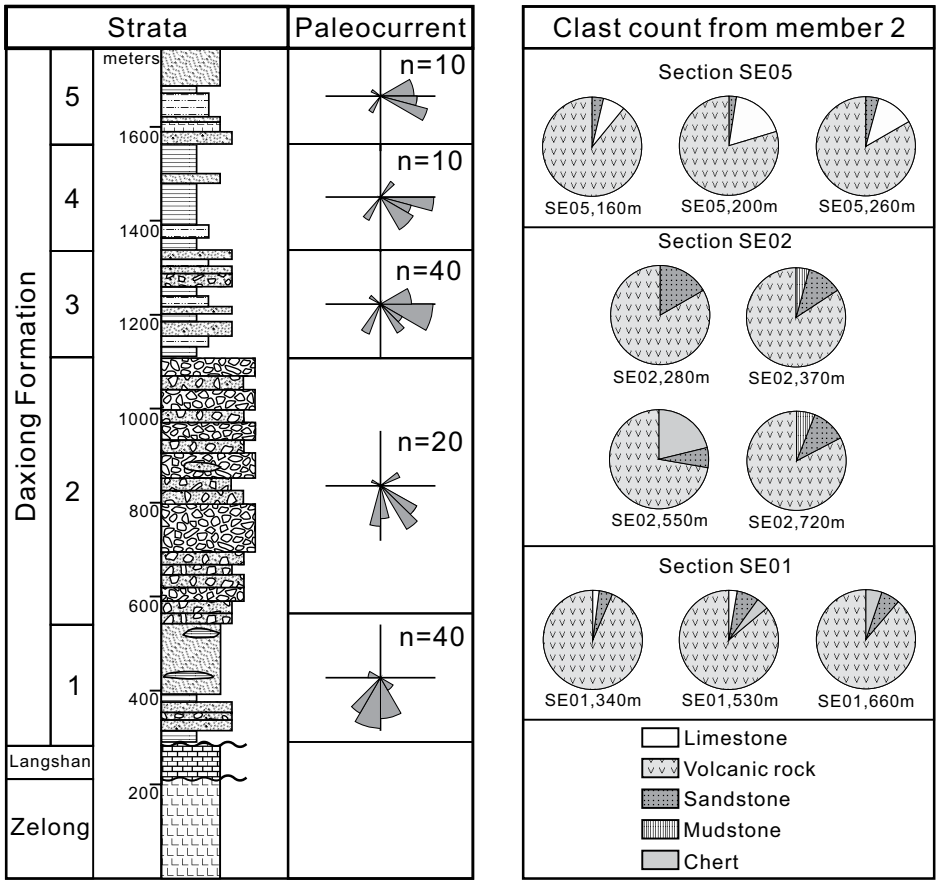

Figure 7. Rose diagrams of paleocurrent directions and pie charts of conglomerate clast compositions. The stratigraphic section and position listed under each pie chart refer to Figure 4. An integrated stratigraphic column is shown on the left.

Member 3

Description. The thickness of this member is at least 250 m in sections SE01 and SE02 and ~330 m in section SE03. The lithofacies assemblage of member 3 is similar to that of member 1 and consists of red, coarse- to medium-grained, laterally overlapping sandstone beds interbedded with siltstone beds. In contrast, the fining-upward packages are slightly thicker than in member 1, typically varying between ~2 and 3 m thick. In every sandstone package, the basal unit is ~10–30 cm thick and comprises very coarse-grained sandstones or pebbly conglomerates with abundant mudstone intraclasts from the underlying beds. This basal unit grades upward into much thicker, medium-grained sandstone beds (~1 m), which have abundant low- and high-angle trough cross-stratification, plane-parallel laminations, and rare current ripples (lithofacies S1, S2, and S4). Red laminated siltstone or mudstone beds occur in the upper part of the sequence (lithofacies F1). The trough and planar cross-stratifications in the sandstone beds indicate an approximately east-southeast–directed paleoflow (Fig. 7).

Interpretation. The middle sandstone lithofacies associations are interpreted as the deposits of laterally migrating sandy braided river channels (Miall, 1978; Lunt and Bridge, 2004; Bridge and Lunt, 2006), which were, on average, deeper (2–3 m) than those of member 1 (<2 m). This sandstone member is characterized by an upward-fining sequence with multilateral and multistory sandstone beds, which are associated with unstable channels, such as sandy braided streams (Bridge and Lunt, 2006). The other details of the lithofacies assemblages are similar to those in member 1.

Member 4

Description. Member 4 is well exposed in section SE03 and comprises nearly 370 m of monotonous red siltstone and minor, lenticular, fine-grained sandstone beds. Cleavage is well developed in the siltstone beds. The sandstone lenses (20–50 cm in thickness) typically contain cross-lamination and horizontal lamination. Carbonate nodules and fossil plant fragments are locally present in the siltstone beds (lithofacies F2). The upper part of this member is characterized by interbedded gray and red siltstone beds, with gray beds more abundant higher in the section (lithofacies F1). In the uppermost part of the succession, fine- to medium-grained tabular sandstone beds (~20–40 cm thick) with slightly erosional basal surfaces, climbing ripple laminations, horizontal laminations, and small-scale (~20 cm) trough cross-stratification (lithofacies S3 and S4) reappear. The paleocurrent data from the trough cross-stratifications of the top sandstone beds indicate a southeast-directed paleoflow (Fig. 7).

Interpretation. The lithofacies assemblage of member 4 is interpreted as a floodplain depositional environment distal from the main channel system. The monotonous red siltstone represents the floodplain with intermittent drying, leading to the precipitation of carbonate (Mack et al., 1993; Kraus, 1999). The discontinuous fine sandstones are consistent with crevasse splays during bankfull levels (Bridge, 2009). The upper sandstone beds with climbing ripple laminations are interpreted as recording increased proximity to a channel system, possibly representing levee deposits (Bridge, 2009).

Member 5

Description. Member 5 is at least 100 m thick. The massive medium-grained, laterally overlapping sandstone beds (0.5–2 m) of this member commonly occur as faint fining-upward sequences. As a whole, the grain size of each sequence remains relatively constant from the bottom to the top. Trough and planar cross-stratifications are widespread. Very coarse and pebbly clasts are locally present at the base of the sandstone beds (lithofacies S2 and S4). Interbedded fine sandstone and siltstone layers are nearly 40–50 cm thick and have small-scale (~10–20 cm) cross- and horizontal laminations with rare carbonate nodules (lithofacies F1). Compared to the lower sandstone members (members 1 and 3), member 5 has few mudstone or siltstone beds and much thicker medium-grained sandstone beds. The paleocurrent data from the trough and planar cross-stratifications indicate an approximately east-southeast–directed paleoflow (Fig. 7).

Interpretation. The lithofacies assemblages of this member are interpreted as having been deposited in laterally migrating fluvial channels. The lack of thick siltstone and relevant crevasse splay deposits suggests the presence of unconfined shallow sandy braided streams (Lunt and Bridge, 2004; Bridge and Lunt, 2006).

AGE CONSTRAINTS

We use the zircon ages of interstratified tuff layers in the uppermost part of the Daxiong Formation (due to the lack of fossils) and micropaleontology in the underlying Langshan Formation limestone to provide a probable depositional age control for the Daxiong Formation.

The *Orbitolina qatarica*, *Conicorbitolina concava*, *Conicorbitolina conica*, and *Orbitolina* sp. observed in the uppermost part of the Langshan Formation indicate an early Cenomanian age (ca. 100–96 Ma; BouDagher-Fadel, 2008, 2013; Appendix Plate S1 [see footnote 1]), which defines the maximum depositional age for the Daxiong Formation. A total of 30 zircon grains from interbedded tuffs from the uppermost portion of the succession yields a single population with a weighted average age of 91.5 ± 0.7 Ma (2σ, MSWD [mean square weighted deviation] = 1.4; Fig. 8), which reflects the age of the upper part of the Daxiong Formation. In addition, the youngest detrital zircons, from the bottom to the top, provide maximum depositional ages of 102 ± 2 Ma (sample 12DX01), 94 ± 4 Ma (12DX06), 93 ± 4 Ma (12DX14), and 92 ± 2 Ma (13XN25), which are consistent with the results of the underlying limestone and tuff beds. Therefore, the Daxiong Formation was most likely deposited between ca. 96 Ma and ca. 91 Ma.

PROVENANCE ANALYSIS: RESULTS AND INTERPRETATION

Provenance Results

Conglomerate Clast Counts and Lithology

Approximately 1000 conglomerate clasts were counted in the measured sections (Fig. 7). The results reveal that the components are mostly volcanic and sandstone clasts, with minor amounts of limestone, mudstone, and chert. The volcanic clasts are dominated by andesites and dacites, in which feldspar phenocrysts and pilotaxitic texture in the matrix are very common (Fig. 6B). These volcanic clasts compose 70%–95% of the total clasts, with an average of 84%. Quartz-rich sandstones represent the other main component and compose an average of ~9% (Fig. 6C). In section SE05, *Orbitolina*-bearing limestone clasts represent nearly 15% of the clasts, which is much more than the proportions of the other sections (Fig. 7). Additionally, other sedimentary rock clasts, including mudstone and chert clasts, account for only a small proportion.

Sandstone Petrography

Sandstones within members 1 and 2 of the Daxiong Formation are poorly sorted, contain mud infill or calcite cement, and feature angular to subrounded grains. These sandstones have average modal compositions of Qt:F:L = 18:23:59 and Qm:F:Lt = 16:23:61 (Appendix Table S1 [see footnote 1]; Fig. 9). Volcanic fragments are the primary components (~60% of total framework grains) and consist of intermediate to felsic volcanic rocks (Figs. 6D, 6E). Sandstone, mudstone, chert, and limestone are also common in these samples. Plagioclase is common and usually altered. The quartz component is dominated by angular to subrounded monocrystalline quartz with minor quantities of

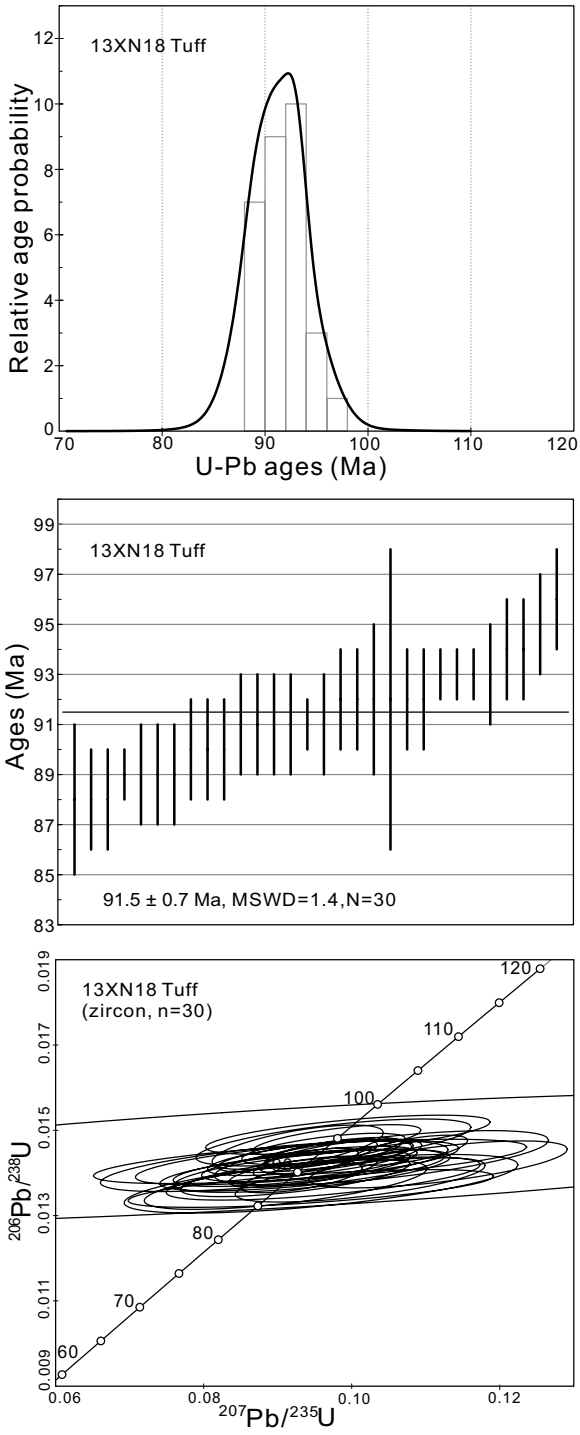

Figure 8. Relative probability and histogram plots of U-Pb zircon ages (upper), weighted mean ages (middle), and concordia diagrams (bottom) of a tuff horizon in the Daxiong Formation (sample 13XN18, from the uppermost part of section SE03).

polycrystalline quartz (only ~1% in total). Epidote and magnetite occur as accessory minerals in these samples.

The sandstone modal framework grains in members 3, 4, and 5 are distinct and have compositions of Qt:F:L = 43:14:43 and Qm:F:Lt = 41:14:45 (Appendix Table S1 [see footnote 1]; Fig. 9). Compared with the lower members, plagioclase is less common and only represents one-quarter of the total grains (Fig. 6F). In contrast, quartz content increases up-section to the same proportion as the lithic fragments, i.e., ~43%. Subangular to well-rounded monocrystalline quartz is common, whereas polycrystalline quartz is rare. Among the lithic fragments, sedimentary fragments increase to a ratio of sedimentary to volcanic fragments of 2:3. The sedimentary fragments are primarily fine quartz sandstone, siltstone, and minor chert, with well- to subrounded textures. The intermediate to felsic volcanic fragments are similar to those in the lower members.

Detrital Zircon U-Pb Ages

In total, 502 detrital zircons from seven sandstones of the Daxiong Formation (as shown in the sedimentary logs of Fig. 4) were dated by LA-ICP-MS. The results reveal that ~80% of the zircon ages range between 92 and 150 Ma, with a peak at ca. 110 Ma (Appendix Table S2 [see footnote 1]; Figs. 10 and 11). Separately, among the 96 valid zircon ages from the basal sandstone of the sequence (sample 12DX01, member 1), 62 zircons yield the youngest age of 102 ± 2 Ma and have a large age population between 102 and 130 Ma (peaking at ca. 115 Ma; Fig. 10). The others (34 zircons) have age ranges of 480–600 Ma and 950–1200 Ma, with peaks at ca. 505 Ma and ca. 1100 Ma, respectively. The 207 zircons from samples 12DX06, 12DX10, and 12DXA10 from member 2 produce a large age population (188 zircons) of 90–120 Ma, with a single peak at 110 Ma. Only 19 zircons from the sample 12DX06 have old ages (>250 Ma) that are similar to those from sample 12DX01, with peaks at ca. 500 Ma and ca. 1100 Ma (Fig. 10). Of the 111 zircons of samples 12DX13 and 12DX14 from member 3, 107 zircons exhibit a dominant age population between 100 and 120 Ma, with a unimodal peak at ca. 110 Ma. The 88 zircons of sample 13XN25 from the top of the sequence (member 5) yield an age distribution similar to that of sample 12DX01 at the bottom, including 54 Mesozoic (age population between 105 and 130 Ma) and 34 pre-Mesozoic ages (age populations of 500–600 Ma and 950–1300 Ma) (Fig. 10).

Detrital Zircon Hf Isotopes

In total, the 255 detrital zircon Hf isotope measurements (age corrected using U-Pb ages from individual zircons) obtained for the dated zircon grains include 196 Mesozoic and 59 pre-Mesozoic ages. Among the 196 Mesozoic zircon Hf isotope measurements, 193 zircons yield low $^{176}Hf/^{177}Hf$ isotopic ratios and negative $\varepsilon_{Hf}(t)$ values between –16.5 and +3.6 (average of –6.8) with T^{C}_{DM} model ages of 2.6–0.9 Ga. The other three Mesozoic zircons exhibit high $^{176}Hf/^{177}Hf$ isotopic ratios and very positive $\varepsilon_{Hf}(t)$ values (+7.0 to +13.6). The 59 pre-Mesozoic zircon Hf

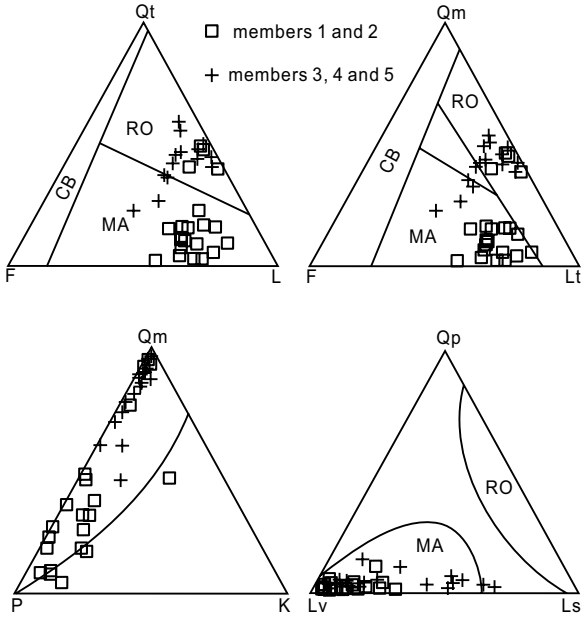

Figure 9. Ternary diagrams of sandstone framework compositions from the Daxiong Formation. CB—continental terrane provenance; RO—recycled orogen provenance; MA—magmatic arc provenance (Dickinson et al., 1983; Garzanti et al., 2007); Qm—monocrystalline quartz; Qp—polycrystalline quartz; L—total nonquartzose lithic grains; Lv—total volcanic lithic grains; Ls—total sedimentary lithic grains; P—plagioclase feldspar; K—potassium feldspar; Qt—total quartz (Qm + Qp); Lt—total lithic grains (L + Qp); F—total feldspar (P + K).

isotopes have a broad $\varepsilon_{Hf}(t)$ value range between –23.4 and +7.3 with T^{C}_{DM} model ages of 3.5–1.3 Ga (Appendix Table S3 [see footnote1]; Fig. 12).

Provenance Interpretation

Zircon Isotopic Properties of the Tibetan Plateau

A comparison of zircon U-Pb ages and Hf isotopes with potential source areas can pinpoint the likely provenance of the sediment. Leier et al. (2007c) compiled published detrital zircon ages of Carboniferous to Cretaceous strata from the Songpan-Ganzi and Kunlun terranes (Fig. 1A), which have age populations of 200–500 Ma and 1700–2000 Ma. These populations contrast with those of the Lhasa terrane, which is characterized by age populations of 50–200 Ma, 500–600 Ma, and 1000–1400 Ma. Numerous zircon ages have been reported from the Cretaceous intrusive and sedimentary rocks in the Bangong-Nujiang suture zone, which display young age populations similar to those of the Lhasa terrane, with an age range of 100–150 Ma (Kapp et al., 2007a; DeCelles et al., 2007b; Zhu et al., 2011a). However, the igneous rocks from the Qiangtang terrane tend to be in the 190–220 Ma age range (Gehrels et al., 2011; Leier et al., 2007c, and references therein), which differs from the Lhasa terrane. Because the southern and northern Lhasa subterranes have similar zircon U-Pb age populations (Leier et al., 2007c; Gehrels et al., 2011), we use the zircon Hf isotopes to distinguish between the two subterranes.

The southern Lhasa subterrane (Gangdese magmatic arc) has experienced substantial magmatism since the Mesozoic. Based on the published data, the 1759 zircons from intrusive and volcanic rocks of the Gangdese magmatic arc exhibit three significant age populations: 39–70 Ma (peaking at ca. 50 Ma), 80–110 Ma (peaking at ca. 90 Ma), and 180–210 Ma (peaking at ca. 190 Ma) (Fig. 11; Chu et al., 2006; Wen et al., 2008; Ji et al., 2009; Zhu et al., 2011a, and references therein). These ages have relatively high $^{176}Hf/^{177}Hf$ isotopic ratios, positive $\varepsilon_{Hf}(t)$ values, and T^{C}_{DM} model ages of 0.3–1.0 Ga (Fig. 12; Chu et al., 2006; Ji et al., 2009). The Xigaze forearc basin is considered to be derived from the Gangdese magmatic arc and has detrital zircon age populations of 75–125 Ma and 150–160 Ma, with age peaks of ca. 90 and ca. 160 Ma, respectively (Fig. 11; Wu et al., 2010; An et al., 2014; Orme et al., 2014). Zircon Hf isotopes of the Xigaze forearc basin record mainly high $^{176}Hf/^{177}Hf$ ratios and positive $\varepsilon_{Hf}(t)$ values with relatively few low $^{176}Hf/^{177}Hf$ isotopic ratios and negative $\varepsilon_{Hf}(t)$ values (Wu et al., 2010; An et al., 2014), which are consistent with the zircons from the Gangdese magmatic arc.

The northern Lhasa subterrane experienced magmatism during the Mesozoic as well, especially during the Early Cretaceous, when numerous intrusive and volcanic rocks were generated (Volkmer et al., 2007; Meng et al., 2010; Zhu et al., 2011a, and references therein). The 761 zircons from the magmatic rocks display Mesozoic ages of 110–140 Ma, with an age peak at ca. 110 Ma (Fig. 11). Approximately 75% of these zircons (572 out of 761 zircons) yield low $^{176}Hf/^{177}Hf$ isotopic ratios, negative $\varepsilon_{Hf}(t)$ values, and T^{C}_{DM} model ages between 1.4 and 2.1 Ga (Fig. 12; Chu et al., 2006; Zhu et al., 2011a), which are distinct from the southern Lhasa zircons. Certain detrital zircons from Cretaceous strata in the Linzhou Basin yield a range of ages between 105 and 140 Ma, with a peak at ca. 120 Ma (Leier et al., 2007b, 2007c). One Paleozoic detrital sample features two age populations: 500–600 Ma (peaking at ca. 540 Ma) and 1050–1300 Ma (peaking at ca. 1120 Ma) (Leier et al., 2007b).

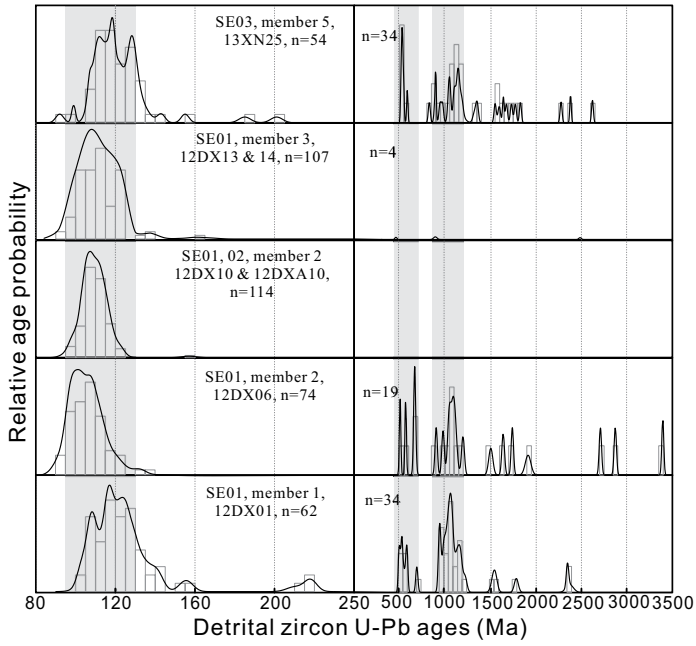

Figure 10. Relative U-Pb age probabilities for detrital zircons from the sandstones of the Daxiong Formation. Note the change in scale at 250 Ma.

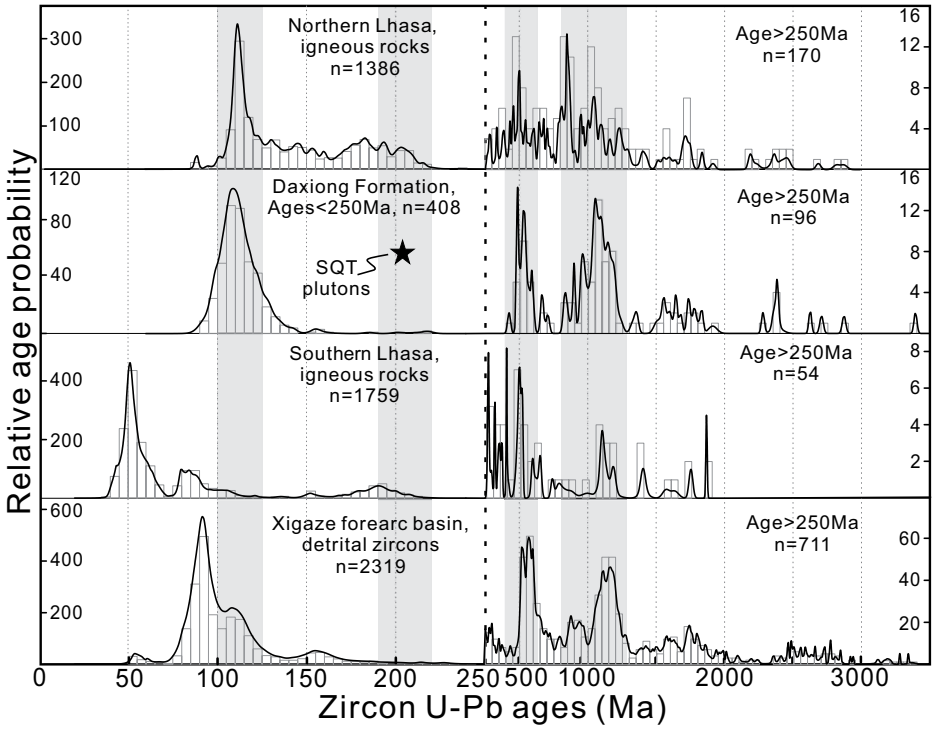

Figure 11. Comparisons of probability density diagrams of detrital zircon ages from the Daxiong Formation (this study) to reference populations from the southern Lhasa subterrane (Zhang et al., 2007a; Lee et al., 2007, 2009; Wen et al., 2008; Chu et al., 2006, 2011; Ji et al., 2009; Zhu et al., 2009, 2011a), northern Lhasa subterrane (Murphy et al., 1997; Chu et al., 2006; Guynn et al., 2006; Zhang et al., 2007b; He et al., 2006a, 2006b; Kapp et al., 2003b, 2005; Liu et al., 2006; Volkmer et al., 2007; Zhou et al., 2008; Meng et al., 2010; Zhu et al., 2009, 2011a), and Xigaze forearc basin (Wu et al., 2010; An et al., 2014; Orme et al., 2014). Note the change of scale at 250 Ma. SQT plutons—southern Qiangtang terrane plutons.

Provenance Interpretation of the Daxiong Formation

Approximately 80% of the analyzed detrital zircons from the Daxiong Formation yield an age population that ranges between 92 and 150 Ma, with a unimodal peak at ca. 110 Ma (Fig. 11). The Hf isotopes from these young zircons display low $^{176}Hf/^{177}Hf$ isotopic ratios and negative $\varepsilon_{Hf}(t)$ values (Fig. 12). Compared with the above potential sources, the age population pattern of the Daxiong Formation is distinctively different from that of the Qiangtang terrane, which tends to be characterized by 190–220 Ma igneous rocks. Similarly, the distinctive age populations of 200–500 Ma in the Songpan-Ganzi and Kunlun terranes are not observed in our data (Leier et al., 2007c). The southern Lhasa subterrane (Gangdese magmatic arc) and the Xigaze forearc basin have similar age populations of 80–110 Ma; however, their extremely high $^{176}Hf/^{177}Hf$ isotopic ratios and positive $\varepsilon_{Hf}(t)$ values differ from those of the zircons of the Daxiong Formation (Wu et al., 2010; An et al., 2014). In contrast, the age populations of the Daxiong Formation are quite similar to those of the northern Lhasa subterrane, with numerous low $^{176}Hf/^{177}Hf$ isotopic ratios, negative $\varepsilon_{Hf}(t)$ values, and similar T^{C}_{DM} model ages (Fig. 12). Therefore, we conclude that the northern Lhasa subterrane was the source area for the Daxiong Formation. Geochronological studies indicate that the Bangong-Nujiang suture zone has zircon age patterns (peaking at ca. 110 Ma) similar to our data. Based on the studies in the southern Nima Basin of the Bangong-Nujiang suture zone, the Gaize–Selin Co thrust uplifted the northern Lhasa subterrane during the Late Cretaceous (Kapp et al., 2007a; DeCelles et al., 2007b). The elevated northern Lhasa subterrane was eroded and provided the source for the southern Nima Basin to the north as well as the Coqen Basin to the south. According to the regional paleogeography during this time (see discussion in "Late Cretaceous paleogeography of the Lhasa terrane"), we believe the sediment from the Bangong-Nujiang suture zone could not have been transported across the Gaize–Selin Co thrust to accumulate in the Coqen Basin by Late Cretaceous time. Furthermore, much of the Daxiong Formation was deposited as debris flows on alluvial fans, which represent short transport distances (usually less than 15 km from the source area; Blair and McPherson, 1994). Approximately southward paleocurrents and intermediate to felsic volcanic clasts are found in our sections. The sandstone modal framework compositions from members 1 and 2 mostly plot in the magmatic arc provenance field. Based on the regional geologic setting, the Lower Cretaceous Zelong Group volcanic rocks, widely exposed in the northern Lhasa subterrane at the time, were the most likely source for the Daxiong Formation. However, there are many limestone clasts present in the conglomerate member (member 2) in section SE05 (Fig. 7). This characteristic reflects the short transport distances of the alluvial fan deposits, in which limestone strata were eroded to form the locally abundant carbonate clasts.

Additionally, sandstone petrography records an increase in quartz grains and sedimentary clasts at the transition from members 1 and 2 to members 3, 4, and 5. The Qt-F-L and Qm-F-Lt diagrams indicate that the sandstones are dominated by the "recycled orogen" fields (Fig. 9) (Dickinson et al., 1983; Garzanti et al., 2007), and the Qm-P-K and Qp-Lv-Ls diagrams indicate an increase in the input of terrestrial recycled rocks. The detrital zircon age patterns from members 3, 4, and 5 yield two additional old age populations (500–600 Ma and 1000–1300 Ma) in addition to the sharp age peak at ca. 110 Ma, which is similar to the published ages from upper Paleozoic strata in the northern Lhasa subterrane (Leier et al., 2007b; Zhu et al., 2011b). Therefore, during this time interval, the source of the deposits was likely recycled debris from a dissected source area and the underlying Paleozoic strata of the northern Lhasa subterrane.

DISCUSSION

Depositional Model for the Daxiong Formation

The sedimentary characteristics of the Daxiong Formation suggest relatively limited transport distances and rapid deposition (greater than 0.3 km m.y.$^{-1}$) in alluvial fans and braided streams. The sandstone petrology, paleoflow directions, and detrital zircon ages and Hf isotopes indicate that the deposition of the Daxiong Formation was related to the erosion of volcanic rocks exposed in proximal areas of the northern Lhasa subterrane. This local sediment source is further supported by the conglomerate clast population, which features abundant poorly sorted, large, subangular volcanic clasts. In the Coqen Basin, thrust deformation exerted an important influence on the deposition of

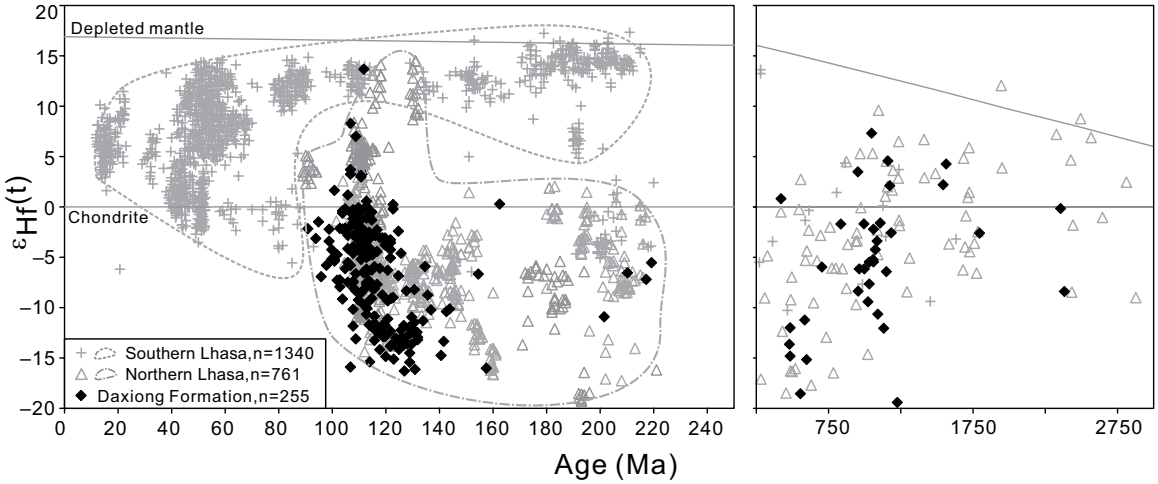

Figure 12. Plots of $\varepsilon_{Hf}(t)$ values versus the U-Pb ages of detrital zircons from sandstones within the Daxiong Formation. Data of the southern Lhasa subterrane are from Chu et al. (2006), Zhang et al. (2007a), Lee et al. (2007), Ji et al. (2009), and Zhu et al. (2009, 2011a); those of the northern Lhasa subterrane are from Chu et al. (2006), Zhang et al. (2007b), and Zhu et al. (2011a).

the Daxiong Formation. The Gugu La thrust elevated the Lower Cretaceous Zelong volcanic rocks in the hanging wall, forming the regional high topography. In this deformational setting, the Daxiong Formation was syn-tectonically deposited at the footwall and received sediment from the overthrust hanging wall. It is possible that a reduction in the thrust activity may have caused the depositional system to evolve from alluvial fans into more discrete channels and floodplains. Therefore, we suggest that the syntectonic depositional processes of the Daxiong Formation can be summarized as follows.

The first stage (member 1) was the result of initial deformation and thrusting, which drove the transition from the shallow marine environment (Langshan Formation) to continental sedimentation in braided rivers. Shallow (<2 m of water depth), laterally migrating, and roughly southward-flowing braided channels developed in the proximal region of the local highlands (Fig. 13A).

The second stage (member 2) features nearly 800 m of conglomerate beds that were deposited in alluvial fans (Fig. 13B). As displacement on the Gugu La thrust increased, the Zelong volcanic rocks in the north of the study area were displaced upward to form the topographically high source area. The low textural maturity and composition (>85% volcanic pebbles) and the unimodal zircon age peak of the sandstones in member 2 indicate that this member was dominantly derived from the elevated Zelong Group volcanic rocks in the hanging wall of the Gugu La thrust.

During the third stage (members 3, 4, and 5), sediment routing became axial relative to the thrust-related topographic high (Fig. 13C), as recorded by the roughly eastward paleoflow directions. Laterally overlapping and lenticular sandstone beds with much thicker sandstone packages indicate deeper (~2–3 m of water depth) migrating fluvial channels, whereas the thick siltstone beds were deposited in the distal floodplain areas of a braided river system.

Late Cretaceous Paleogeography of the Lhasa Terrane

Due to the northward subduction of the Neotethyan oceanic slab and Lhasa-Qiangtang terrane collision, several sedimentary basins developed in the Lhasa terrane during the Late Cretaceous. Here, we compare the contemporaneous basins of the Lhasa terrane in order to restore the Late Cretaceous paleogeography and depositional framework of the region (Fig. 13D; Fig. 14).

The Xigaze forearc basin was located between the Indus-Yarlung suture zone and the Gangdese magmatic arc and accumulated thousands of meters of a range of Albian–Campanian deep-water submarine fan turbidites to delta deposits (Dürr, 1996; Wang et al., 2012; An et al., 2014; Orme et al., 2014). The Gangdese magmatic arc was the dominant source area for this basin (Wu et al., 2010; Orme et al., 2014). Recently, detrital zircon Hf isotopes from the Xigaze forearc basin have revealed that the northern Lhasa subterrane could also have provided sediments after ca. 88 Ma, which implies that the northern Lhasa subterrane would have been an erosional landscape by ca. 88 Ma. This condition would also imply that the southward-flowing rivers cut across the Gangdese arc to link the northern Lhasa subterrane to the Xigaze forearc basin (An et al., 2014). In the north of the Gangdese magmatic arc, the Late Cretaceous Linzhou Basin accumulated >2000 m of the Takena Formation. The lower part (Penbo member of the Takena Formation) is interpreted to have been deposited in a shallow marine seaway and is overlain by multistory-multilateral braided streams (Lhunzhub member of the Takena Formation) in the upper part (Leier et al., 2007a). Through the integration of the provenance analysis, basin subsidence, and the location of the regional fold-and-thrust belt (Kapp et al., 2007b), the Linzhou Basin has been interpreted as a retroarc foreland basin north of the Gangdese magmatic arc (Leier et al., 2007a). The southern Nima and Selin Co Basins, located on the northern margin of the northern Lhasa subterrane, were strongly influenced by the activity of the Gaize–Selin Co thrust during Late Cretaceous time (Kapp et al., 2007a). The Upper Cretaceous Jingzhushan conglomerate was mostly derived from the Langshan limestone in the hanging wall of the Gaize–Selin Co thrust (DeCelles et al., 2007b; Zhang et al., 2012).

Based on previous work and the results of this study, the northern Lhasa subterrane accumulated the widespread, shallow, *Orbitolina*-rich Langshan limestone during Aptian–early Cenomanian time (Zhang, 2000; Zhang et al., 2004). The formation of this limestone may record large-wavelength subsidence associated with oceanic slab subduction and mantle flow comparable to the Western Interior Seaway of North America (Murphy et al., 1997; Leier et al., 2007a). Subsequently, the northern Lhasa subterrane accumulated the terrestrial clastic rocks of the Daxiong Formation. In the Coqen

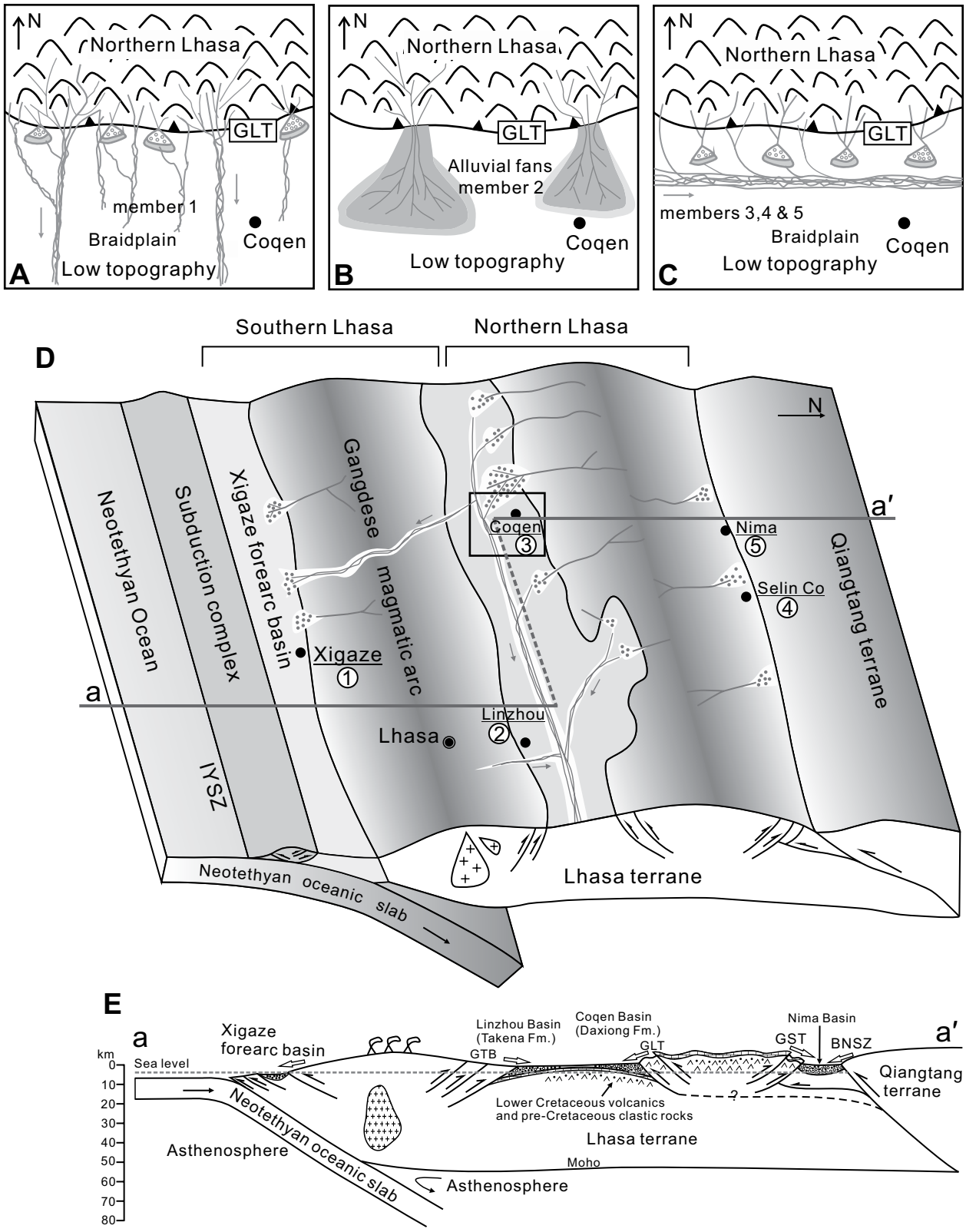

Figure 13. (A–C) Sketched maps for the different depositional stages of the Daxiong Formation. (D) Simplified Late Cretaceous paleogeography and geomorphology of the Lhasa terrane during ca. 96–91 Ma. Numbered circles are basin locations referred to in Figure 14. Not drawn to scale. (E) Schematic south-north cross section (a-a′ shown in D) illustrating the hypothetical tectonic model of the Late Cretaceous sedimentary basins in the Lhasa terrane. BNSZ—Bangong-Nujiang suture zone; GST—Gaize–Selin Co thrust; GLT—Gugu La thrust; GTB—Gangdese retroarc thrust belt; IYSZ—Indus-Yarlung Suture Zone.

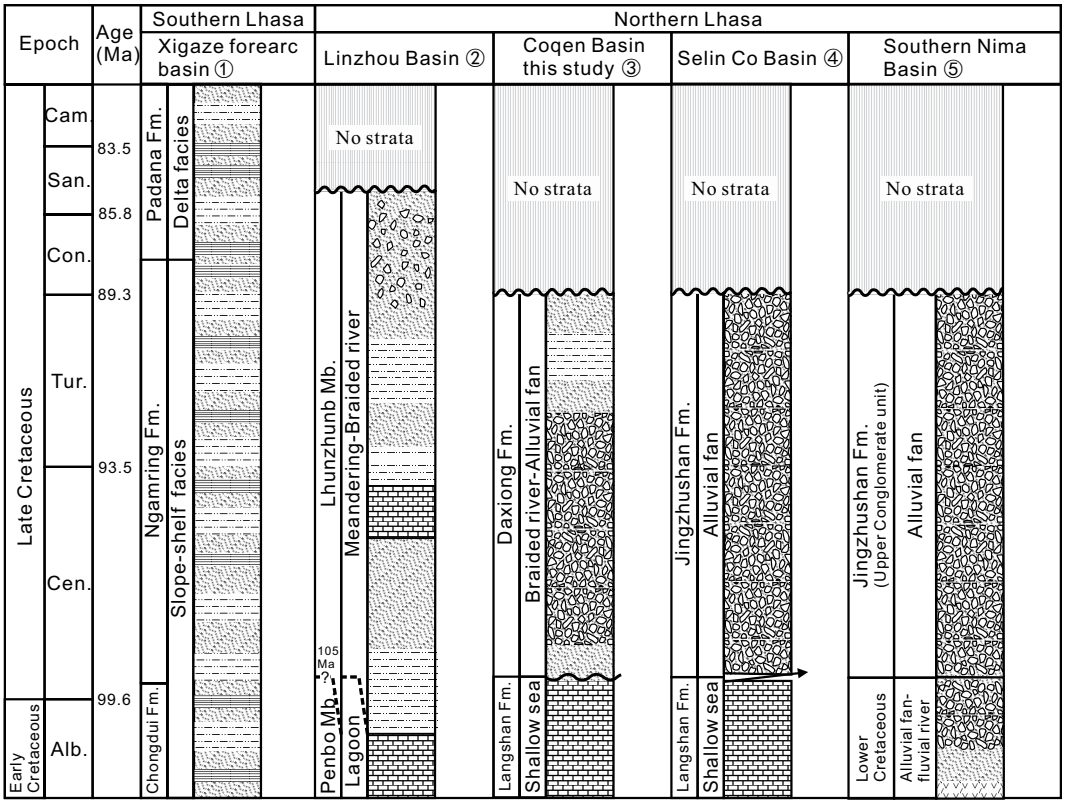

Figure 14. Comparisons of the Cretaceous strata in the Xigaze forearc basin, Linzhou Basin, southern Nima Basin, Selin Co Basin, and Coqen Basin (this study). The strata and time scale in ordinate are referred to in An et al. (2014), Leier et al. (2007a), DeCelles et al. (2007b), and Zhang et al. (2012). See Figure 4 for the lithological legend, and Figure 13D for the basin locations. Alb.—Albian; Cen.—Cenomanian; Tur.—Turonian; Con.—Coniacian; San.—Santonian; Cam.—Campanian.

Basin, a roughly southward and eastward fluvial system developed and was sourced from the northern Lhasa subterrane. Simultaneously, the southern Lhasa subterrane (Gangdese magmatic arc) served as a source for both the Linzhou retroarc foreland basin to the north and the Xigaze forearc basin to the south (Leier et al., 2007a; Wu et al., 2010; An et al., 2014). The Xigaze forearc basin was still close to sea level and received sediment from the northern Lhasa subterrane at ca. 88 Ma (Dürr 1996; Wang et al., 2012; An et al., 2014). Therefore, during Late Cretaceous time (approximately post–88 Ma), there must have been a southward-flowing river that cut across the Gangdese magmatic arc and that originated from the northern Lhasa subterrane, which fed both the Daxiong Formation and the Xigaze forearc basin (Fig. 13D). This scenario can be compared to the Rocky Mountain area in the Cordilleran orogen belt of North America, in which the westward "Tyee" paleoriver cut across the Cordilleran magmatic arc to reach the Pacific Ocean during the mid-Eocene (Dickinson et al., 1988).

Tectonic Controls on the Coqen Basin

As previously outlined, at least two tectonic models have been proposed for Late Cretaceous basin evolution in the northern Lhasa subterrane. A peripheral foreland basin was proposed to be the result of crustal loading along the accretionary suture during Lhasa-Qiangtang collision (Leeder et al., 1988; Murphy et al., 1997). Another model was proposed by Leier et al. (2007a), who suggested that the contemporaneous Takena Formation in the Linzhou Basin records a retroarc foreland basin developed to the north of Cretaceous Gangdese fold-and-thrust belt (e.g., GTB in Fig. 13E; Kapp et al., 2007b).

Any tectonic model of the tectonic evolution of the Late Cretaceous Coqen Basin in the northern Lhasa subterrane must account for the following: (1) the Langshan and Daxiong Formations may have been influenced by the subduction of Neotethyan oceanic slab to the south and the Lhasa-Qiangtang collision to the north; (2) the Daxiong Formation unconformably overlies the widespread upper Aptian to lower Cenomanian Langshan limestone; (3) the Daxiong Formation records syn-tectonic deposition linked to a south-directed thrust (Gugu La thrust); (4) the terrestrial alluvial fan and braided river environments of the Daxiong Formation suggest short transport distances, rapid accumulation, and localized source areas; and (5) the Daxiong Formation was mostly sourced from the Lower Cretaceous Zelong volcanic rocks and pre-Cretaceous strata in the northern Lhasa subterrane instead of the southern Gangdese magmatic arc.

The provenance derived from the northern Lhasa subterrane indicates that the Coqen Basin is inconsistent with a retroarc foreland basin related to the Gangdese magmatic arc (Leier et al., 2007a). Therefore, synthesizing the observations in this study, we present a new tectonic model for the Late Cretaceous Coqen Basin in the northern Lhasa subterrane.

During the late Aptian to early Cenomanian (ca. 113–96 Ma), the northward subduction of the Neotethyan oceanic slab commenced along the southern margin of the Lhasa terrane, and an "Andean-style" convergent margin developed (e.g., Allégre et al., 1984; England and Searle, 1986; Fielding, 1996). The Langshan Formation stretched from the Gaize–Selin Co thrust in the north to the Gangdese magmatic arc in the south (Kapp et al., 2005). The Langshan limestone is proposed to record a widespread marine incursion driven by the northward subduction of the Neotethyan oceanic slab (Leier et al., 2007a; DeCelles et al., 2007b).

During the Late Cretaceous (Cenomanian to Turonian, ca. 96–91 Ma), the Coqen Basin developed between the Gangdese magmatic arc to the south and the northern Lhasa subterrane to the north. The Daxiong Formation contains sediment sourced from the local topography of

the northern Lhasa subterrane and was influenced by syn-depositional deformation. Based on our current understanding of the Late Cretaceous Coqen Basin, we suggest that it should be described as a foreland basin without assigning any specific controls other than flexure during thrusting on the Gugu La thrust and loading by the northern Lhasa subterrane (Fig. 13E).

Although sediment delivery to the Coqen Basin was locally derived from the northern Lhasa subterrane, this does not exclude the possibility that the deformation was linked to the growth of the fold-and-thrust belt that resulted from the Lhasa-Qiangtang collision along the Bangong-Nujiang suture zone. In this situation, the Nima Basin can be considered a wedge-top depocenters, and the Coqen Basin would have been the foredeep to a peripheral foreland basin system (DeCelles and Giles, 1996) associated with the Lhasa-Qiangtang collision (Leeder et al., 1988; Murphy et al., 1997).

The tectonic framework for the Coqen Basin is comparable with many intramontane basins in the Central Andes, such as the Altiplano Basin in Bolivia. During mid-Paleocene to early Oligocene times, the Altiplano region was a retroarc foreland basin that was principally sourced from the Western Cordillera magmatic arc (Horton et al., 2001, 2002; DeCelles and Horton, 2003). In the late Oligocene, the Pacific plate subducted more rapidly eastward beneath the Andes range, causing back-thrusts to the east of the Altiplano (Leier et al., 2013; Garzione et al., 2014) and resulting in a north-south–trending plateau characterized by an internal drainage system. This basin accumulated ~3 km of upper Oligocene conglomerate beds, which were mostly sourced from the thrust belt to the east (Horton et al., 2002; Leier et al., 2010). These depositional and tectonic setting characteristics of the late Oligocene Altiplano Basin have been referred to as a "hinterland basin" (Horton et al., 2002; Horton, 2012; Leier et al., 2010).

The Daxiong Formation in the Coqen Basin is broadly similar to the late Oligocene Altiplano Basin in its tectonic framework. However, by Late Cretaceous time, the Coqen Basin was influenced not only by subduction from the south but also by the Lhasa-Qiangtang collision to the north. If the deformation front (the Gugu La thrust) that controlled the northern margin of the Coqen Basin was mechanically linked to the Neotethyan oceanic slab subduction, the likely drivers of subsidence may have been comparable to those of the Altiplano Basin. Alternatively, if the deformation was related to the Lhasa-Qiangtang collision to the north, the Coqen Basin could be considered a peripheral foreland basin driven by the growth of the fold-and-thrust belt.

Implications for the Early Uplift of the Northern Lhasa Subterrane

Many interpretations attempting to constrain the early uplift of the Tibetan Plateau have been published, and these interpretations vary in time and space (Harrison et al., 1992; Murphy et al., 1997; Chung et al., 1998; Rowley and Currie, 2006; DeCelles et al., 2007a; Wang et al., 2008, 2014a; Dai et al., 2012, 2013; Xu et al., 2013; Ding et al., 2014; Staisch et al., 2014). Throughout the Cretaceous, the Lhasa terrane was influenced by Neotethyan oceanic slab subduction prior to the India-Asia collision (Ding et al., 2003; Zhang et al., 2004; Kapp et al., 2005). Furthermore, the Neotethyan slab may have experienced flat-slab subduction beneath the Lhasa terrane, thereby initiating substantial crustal thickening, elevation gain, and the development of related sedimentary basins in the northern Lhasa subterrane (Murphy et al., 1997; Kapp et al., 2005, 2007a; Volkmer et al., 2007; DeCelles et al., 2007b; Ma et al., 2013a, 2013b, 2013c). In this tectonic framework, Late Cretaceous contractional deformation developed in the northern Lhasa subterrane (Murphy et al., 1997; Volkmer et al., 2007; Kapp et al., 2007a), resulting in the growth of topography in the interior region, which was drained by alluvial fans and braided rivers to the north and south (e.g., Jingzhushan Formation in the Selin Co Basin; Zhang et al., 2012). Detritus in the Xigaze forearc basin is confirmed to have been partially derived from the northern Lhasa subterrane after ca. 88 Ma (An et al., 2014), implying a broad distribution of sediment routing in the region.

The Late Cretaceous uplift of the northern Lhasa subterrane is also supported by petrological studies. Several Mg-rich and adakitic volcanic rocks with ages of ca. 93–86 Ma exist in the northern Lhasa subterrane. These volcanics are related to crustal thickening and lower lithospheric delamination following the Early Cretaceous Lhasa-Qiangtang terrane amalgamation (Ma and Yue, 2010; Yu et al., 2011; Yao et al., 2013; Wang et al., 2013; Li et al., 2013; Wang et al., 2014b).

No sedimentary rocks between the uppermost Daxiong Formation and the overlying Cenozoic Linzizong volcanic rocks (e.g., ca. 65–44 Ma; Liu et al., 2004; Mo et al., 2008; Lee et al., 2009) have been preserved. It is unknown whether this ~30 m.y. time gap is related to a depositional hiatus or post-depositional erosion. However, both possibilities suggest that the Late Cretaceous Coqen Basin was post-depositionally uplifted relative to the topographic growth of northern Lhasa subterrane to the north, which further implies the early uplift of southern Tibet. Similarly, there is a ~50 m.y. gap (from ca. 90 to ca. 40 Ma) documented in the southern Nima Basin (DeCelles et al., 2007b). Furthermore, in the Linzhou Basin, the undeformed Cenozoic Linzizong volcanic rocks unconformably overlie the deformed Upper Cretaceous strata, which reflects ~40% upper crustal shortening and thickening during the Late Cretaceous (England and Searle, 1986; Pan, 1993). Actually, this unconformity is apparently widespread from west to east in the southern-central Lhasa subterrane (Murphy et al., 1997; Leier et al., 2007a; Kapp et al., 2007a). Collectively, we conclude that the deposition of the Daxiong Formation was accompanied by crustal thickening and shortening that reflects the initial uplift and growth of the northern Lhasa subterrane in southern Tibet. Paleoaltimetry studies in the Nima Basin (DeCelles et al., 2007a) and southern Qiangtang terrane (Xu et al., 2013) indicate that the central Tibetan Plateau reached elevations of at least 4000 m by the late Oligocene (ca. 28–26 Ma). However, further paleoaltimetry is required to quantify how much of the present elevation of the Tibetan Plateau was reached prior to the India-Asia collision.

CONCLUSIONS

The Langshan and Daxiong Formations in the Coqen Basin in the southern part of the northern Lhasa subterrane record the evolution of the Lhasa terrane during the Late Cretaceous. Based on this study, we have reached the following conclusions.

(1) The Langshan limestone was deposited in a shallow marine setting during ca. 113–96 Ma. The Daxiong Formation was deposited by alluvial fans and braided river systems from ca. 96 Ma to at least ca. 91 Ma, and this formation records the transition from a shallow sea (Langshan Formation) to a terrestrial environment on the northern Lhasa subterrane.

(2) Detrital zircon U-Pb ages, Hf isotopes, and paleocurrent data indicate that the Daxiong Formation was derived from the northern Lhasa subterrane rather than the southern Lhasa subterrane (Gangdese magmatic arc).

(3) The Daxiong Formation was bounded by the Gangdese magmatic arc to the south and the northern Lhasa thrust ridges to the north. The basin setting for the Daxiong Formation was likely a local foreland basin linked to the south-directed thrusting of the northern Lhasa subterrane during the Late Cretaceous. The syn-depositional Gugu La thrust that bounds the northern margin of the basin resulted from crustal stresses generated by Neotethyan oceanic slab subduction and/or Lhasa-Qiangtang collision.

(4) During Late Cretaceous time, the northern Lhasa subterrane experienced crustal shortening and thickening and provided sediment to both sides of the range (e.g., the Coqen Basin and southern Nima Basin). The Upper Cretaceous Daxiong Formation records the initial uplift of the northern Lhasa subterrane.

ACKNOWLEDGMENTS

We appreciate that Bin Wu, Anjun Lin, Zhiyong Zhu, Xiong Yan, Juan Li, and Xuan Lv provided much help in analyzing the zircon U-Pb ages and Hf isotopes. We thank Zhong Han and Wei Zhang for their assistance in the field. This study was financially supported by the Ministry of Science and Technology of the People's Republic of China 973 Project (2012CB822001), the Strategic Priority Research Program (B) of the Chinese Academy of Sciences (XDB03010106), and the National Natural Science Foundation of China Project (41472081, 41172129). We are grateful to Zhengxiang Li (Associate Editor), Peter DeCelles, Andrew Leier, and Eduardo Garzanti for their critical and constructive reviews.

REFERENCES CITED

Allégre, C.J., Courtillot, V., Tapponier, P., Him, A., Mattauer, M., Coulon, C., Jaeger, J.J., Achache, J., Schaerer, U., Marcoux, J., Burg, J.P., Girardeau, J., Armijo, R., Gariepy, C., Coepel, C., Li, T., Xiao, X., Chang, C., Li, G., Lin, B., Teng, J.W., Wang, N., Chen, G., Han, T., Wang, X., Den, W., Sheng, H., Cao, Y., Zhou, J., Qui, H., Bao, P., Wang, S., Wang, B., Zhou, Y., and Ronghua, X., 1984, Structure and evolution of the Himalaya-Tibet orogenic belt: Nature, v. 307, p. 17–22, doi:10.1038/307017a0.

An, W., Hu, X., Garzanti, E., Marcelle, M.K., Wang, J., and Sun, G., 2014, Xigaze forearc basin revisited (South Tibet): Provenance changes and origin of the Xigaze Ophiolite: Geological Society of America Bulletin, v. 126, p. 1595–1613, doi:10.1130/B31020.1.

An, Z.S., Kutzbach, J.E., Prell, W.L., and Porter, S.C., 2001, Evolution of Asian monsoons and phased uplift of the Himalaya–Tibetan Plateau since Late Miocene times: Nature, v. 411, p. 62–66, doi:10.1038/35075035.

Andersen, T., 2002, Correction of common lead in U-Pb analyses that do not report ^{204}Pb: Chemical Geology, v. 192, p. 59–79, doi:10.1016/S0009-2541(02)00195-X.

Blair, T.C., and McPherson, J.G., 1994, Alluvial fans and their natural distinction from rivers based on morphology, hydraulic processes, sedimentary processes, and facies assemblages: Journal of Sedimentary Research, v. 64, p. 450–489.

BouDagher-Fadel, M.K., 2008, Evolution and Geological Significance of Larger Benthic Foraminifera: Developments in Paleontology and Stratigraphy, Volume 21: Amsterdam, Elsevier, 540 p.

BouDagher-Fadel, M.K., 2013, Biostratigraphic and Geological Significance of Planktonic Foraminifera, 2nd edition: London, UK, Office of the Vice Provost Research (OVPR), University College, 307 p.

Bouvier, A., Vervoort, J.D., and Patchett, P.J., 2008, The Lu-Hf and Sm-Nd isotopic composition of CHUR: Constraints from unequilibrated chondrites and implications for the bulk composition of terrestrial planets: Earth and Planetary Science Letters, v. 273, p. 48–57, doi:10.1016/j.epsl.2008.06.010.

Bridge, J.S., 2009, Rivers and Floodplains: Forms, Processes, and Sedimentary Record: Oxford, UK, Blackwell, 487 p.

Bridge, J.S., and Lunt, I.A., 2006, Depositional models of braided rivers, *in* Sambrook Smith, G.H., Best, J.L., Bristow, C.S., and Petts, G., eds., Braided Rivers II: Oxford, UK, Blackwell, p. 11–50.

Bristow, C.S., 1993, Sedimentary structures exposed in bar tops in the Brahmaputra River, Bangladesh, *in* Best, J.L., and Bristow, C.S., eds., Braided Rivers: Geological Society of London Special Publication 75, p. 277–290.

Burg, J.P., Proust, F., Tapponnier, P., and Chen, G.M., 1983, Deformation phases and tectonic evolution of the Lhasa block, China: Eclogae Geologicae Helvetiae, v. 76, p. 643–665.

Cawood, P.A., Hawkesworth, C.J., and Dhuime, B., 2012, Detrital zircon record and tectonic setting: Geology, v. 40, p. 875–878, doi:10.1130/G32945.1.

Cheng, J., and Xu, G., 1986, Geologic map of the Gaize region with report: Chengdu, Tibetan Bureau of Geology and Mineral Resources, 369 p., scale 1:1,000,000.

Cheng, J., and Xu, G., 1987, Geologic map of the Ritu region with report: Chengdu, Tibetan Bureau of Geology and Mineral Resources, 598 p., scale 1:1,000,000.

Chu, M., Chung, S., Song, B., Liu, D., O'Reilly, S., Pearson, N., Ji, J., and Wen, D., 2006, Zircon U-Pb and Hf isotope constraints on the Mesozoic tectonics and crustal evolution of southern Tibet: Geology, v. 34, p. 745–748, doi:10.1130/G22725.1.

Chu, M., Chung, S., O'Reilly, S., Pearson, N., Wu, F., Li, X., Liu, D., Ji, J., Chu, C., and Lee, H., 2011, India's hidden inputs to Tibetan orogeny revealed by Hf isotopes of Transhimalayan zircons and host rocks: Earth and Planetary Science Letters, v. 307, p. 479–486, doi:10.1016/j.epsl.2011.05.020.

Chung, S., Lo, C., Lee, T., Zhang, Y., Xie, Y., Li, X., Wang, K., and Wang, P., 1998, Diachronous uplift of the Tibetan plateau starting 40 Myr ago: Nature, v. 394, p. 769–773, doi:10.1038/29511.

Dai, J., Zhao, X., Wang, C., Zhu, L., Li, Y., and Finn, D., 2012, The vast proto–Tibetan Plateau: New constraints from Paleogene Hoh Xil Basin: Gondwana Research, v. 22, p. 434–446, doi:10.1016/j.gr.2011.08.019.

Dai, J., Wang, C., Hourigan, J., Li, Z., and Zhuang, G., 2013, Exhumation history of the Gangdese Batholith, southern Tibetan Plateau: Evidence from apatite and zircon (U-Th)/He thermochronology: The Journal of Geology, v. 121, p. 155–172, doi:10.1086/669250.

DeCelles, P.G., and Giles, K.A., 1996, Foreland basin systems: Basin Research, v. 8, p. 105–123, doi:10.1046/j.1365-2117.1996.01491.x.

DeCelles, P.G., and Horton, B.K., 2003, Early to middle Tertiary foreland basin development and the history of Andean crustal shortening in Bolivia: Geological Society of America Bulletin, v. 115, p. 58–77, doi:10.1130/0016-7606(2003)115<0058:ETMTFB>2.0.CO;2.

DeCelles, P.G., Langford, R.P., and Schwartz, R.K., 1983, Two new methods of paleocurrent determination from trough cross-stratification: Journal of Sedimentary Petrology, v. 53, p. 629–642.

DeCelles, P.G., Gray, M.B., Cole, R.B., Pequera, N., Pivnik, D.A., Ridgway, K.D., and Srivastava, P., 1991, Controls on synorogenic alluvial-fan architecture, Beartooth Conglomerate (Palaeocene), Wyoming and Montana: Sedimentology, v. 38, p. 567–590, doi:10.1111/j.1365-3091.1991.tb01009.x.

DeCelles, P.G., Quade, J., Kapp, P., Fan, M., Dettman, D.L., and Ding, L., 2007a, High and dry in central Tibet during the late Oligocene: Earth and Planetary Science Letters, v. 253, p. 389–401, doi:10.1016/j.epsl.2006.11.001.

DeCelles, P.G., Kapp, P., Ding, L., and Gehrels, G.E., 2007b, Late Cretaceous to mid-Tertiary basin evolution in the central Tibetan Plateau: Changing environments in response to tectonic partitioning, aridification, and regional elevation gain: Geological Society of America Bulletin, v. 119, p. 654–680, doi:10.1130/B26074.1.

DeCelles, P.G., Kapp, P., Gehrels, G.E., and Ding, L., 2014, Paleocene-Eocene foreland basin evolution in the Himalaya of southern Tibet and Nepal: Implications for the age of initial India-Asia collision: Tectonics, v. 33, p. 824–849, doi:10.1002/2014TC003522.

Dewey, J.F., Shackleton, R.M., Chang, C., and Yiyin, S., 1988, The tectonic evolution of the Tibetan Plateau: Philosophical Transactions of the Royal Society of London, Series A, Mathematical and Physical Sciences, v. 327, p. 379–413, doi:10.1098/rsta.1988.0135.

Dickinson, W., and Gehrels, G., 2009, Use of U-Pb ages of detrital zircons to infer maximum depositional ages of strata: A test against a Colorado Plateau Mesozoic database: Earth and Planetary Science Letters, v. 288, p. 115–125, doi:10.1016/j.epsl.2009.09.013.

Dickinson, W.R., Beard, S.L., Brakenridge, G.R., Erjavec, J.L., Ferguson, R.C., Inman, K.F., Knepp, R.A., Lindberg, F.A., and Ryberg, P.T., 1983, Provenance of North American Phanerozoic sandstones in relation to tectonic setting: Geological Society of America Bulletin, v. 94, p. 222–235, doi:10.1130/0016-7606(1983)94<222:PONAPS>2.0.CO;2.

Dickinson, W.R., Klute, M.A., Hayes, M.J., Janecke, S.U., Lundin, E.R., McKittrick, M.A., and Olivares, M.D., 1988, Paleogeographic and paleotectonic setting of Laramide sedimentary basins in the central Rocky Mountain region: Geological Society of America Bulletin, v. 100, p. 1023–1039, doi:10.1130/0016-7606(1988)100<1023:PAPSOL>2.3.CO;2.

Ding, L., Kapp, P., Zhong, D., and Deng, W., 2003, Cenozoic volcanism in Tibet: Evidence for a transition from oceanic to continental subduction: Journal of Petrology, v. 44, p. 1833–1865, doi:10.1093/petrology/egg061.

Ding, L., Xu, Q., Yue, Y.H., Wang, H.Q., Cai, F.L., and Li, S., 2014, The Andean-type Gangdese Mountains: Paleoelevation record from the Paleocene–Eocene Linzhou Basin: Earth and Planetary Science Letters, v. 392, p. 250–264, doi:10.1016/j.epsl.2014.01.045.

Dürr, S.B., 1996, Provenance of Xigaze forearc clastic rocks (Cretaceous, south Tibet): Geological Society of America Bulletin, v. 108, p. 669–684, doi:10.1130/0016-7606(1996)108<0669:POXFAB>2.3.CO;2.

England, P., and Searle, M., 1986, The Cretaceous-Tertiary deformation of the Lhasa block and its implications for crustal thickening in Tibet: Tectonics, v. 5, p. 1–14, doi:10.1029/TC005i001p00001.

Fielding, E.J., 1996, Tibet uplift and erosion: Tectonophysics, v. 260, p. 55–84, doi:10.1016/0040-1951(96)00076-5.

Garzanti, E., Doglioni, C., Vezzoli, G., and Ando, S., 2007, Orogenic belts and orogenic sediment provenance: The Journal of Geology, v. 115, p. 315–334, doi:10.1086/512755.

Garzione, C.N., Auerbach, D.J., Smith, J., Rosario, J.J., Passey, B.H., Jordan, T.E., and Eiler, J.M., 2014, Clumped isotope evidence for diachronous surface cooling of the Altiplano and pulsed surface uplift of the Central Andes: Earth and Planetary Science Letters, v. 393, p. 173–181, doi:10.1016/j.epsl.2014.02.029.

Gehrels, G., Kapp, P., DeCelles, P., Pullen, A., Blakey, R., Weislogel, A., Ding, L., Guynn, J., Martin, A., Mcquarrie, N., and Yin, A., 2011, Detrital zircon geochronology of pre-Tertiary strata in the Tibetan-Himalayan orogen: Tectonics, v. 30, TC5016, doi:10.1029/2011TC002868.

Griffin, W.L., Wang, X., Jackson, S.E., Pearson, N.J., and O'Reilly, S.Y., 2002, Zircon geochemistry and magma mixing, SE China: In-situ analysis of Hf isotopes, Tonglu and Pingtan igneous complexes: Lithos, v. 61, p. 237–269, doi:10.1016/S0024-4937(02)00082-8.

Guynn, J.H., Kapp, P., Pullen, A., Heizler, M., Gerhels, G.E., and Lin, D., 2006, Tibetan basement rocks near Amdo reveal "missing" Mesozoic tectonism along the Bangong suture, central Tibet: Geology, v. 34, p. 505–508, doi:10.1130/G22453.1.

Harrison, T.M., Copeland, P., Kidd, W.S.F., and Yin, A., 1992, Raising Tibet: Science, v. 255, p. 1663–1670, doi:10.1126/science.255.5052.1663.

He, S., Kapp, P., DeCelles, P.G., Gehrels, G.E., and Heizler, M., 2007, Cretaceous–Tertiary geology of the Gangdese Arc in the Linzhou area, southern Tibet: Tectonophysics, v. 433, p. 15–37, doi:10.1016/j.tecto.2007.01.005.

He, Z.H., Yang, D.M., and Wang, T.W., 2006a, The determination of Early Cretaceous post-collision granitoids in Sangba area of Gangdese tectonic belt and its tectonic significance [in Chinese with English abstract]: Acta Petrologica et Mineralogica, v. 25, p. 185–193.

He, Z.H., Yang, D.M., Zheng, C.Q., and Wang, T.W., 2006b, Isotopic dating of the Mamba granitoid in the Gangdise tectonic belt and its constraint on the subduction time of the Neotethys [in Chinese with English abstract]: Geological Review, v. 52, p. 100–106.

He, Z.Y., Xu, X.S., Zou, H.B., Wang, X.D., and Yu, Y., 2010, Geochronology, petrogenesis and metallogeny of Piao-

tang granitoids in the tungsten deposit region of south China: Geochemical Journal, v. 44, p. 299–313.

Hetzel, R., Dunkl, I., Haider, V., Strobl, M., von Eynatten, H., Ding, L., and Frei, D., 2011, Peneplain formation in southern Tibet predates the India-Asia collision and plateau uplift: Geology, v. 39, p. 983–986, doi:10.1130/G32069.1.

Horton, B.K., 2012, Cenozoic evolution of hinterland basins in the Andes and Tibet, *in* Busby, C., and Azor, A., eds., Tectonics of Sedimentary Basins: Oxford, UK, Blackwell, Recent Advances, 664 p.

Horton, B.K., Hampton, B.A., and Waanders, G.L., 2001, Paleogene synorogenic sedimentation in the Altiplano plateau and implications for initial mountain building in the central Andes: Geological Society of America Bulletin, v. 113, p. 1387–1400, doi:10.1130/0016-7606(2001)113<1387:PSSITA>2.0.CO;2.

Horton, B.K., Hampton, B.A., Lareau, B.N., and Baldellon, E., 2002, Tertiary provenance history of the Northern and Central Altiplano (central Andes, Bolivia): A detrital record of plateau-margin tectonics: Journal of Sedimentary Research, v. 72, p. 711–726, doi:10.1306/020702720711.

Hu, X.M., Sinclair, H.D., Wang, J.G., Jiang, H.H., and Wu, F.Y., 2012, Late Cretaceous–Palaeogene stratigraphic and basin evolution in the Zhepure Mountain of southern Tibet: Implications for the timing of India-Asia initial collision: Basin Research, v. 24, p. 520–543, doi:10.1111/j.1365-2117.2012.00543.x.

Ingersoll, R.V., Bullard, T.F., Ford, R.L., Grimm, J.P., Pickle, J.D., and Sares, S.W., 1984, The effect of grain size on detrital modes: A test of the Gazi-Dickinson point-counting method: Journal of Sedimentary Petrology, v. 54, p. 103–116.

Jackson, S.E., Pearson, N.J., Griffin, W.L., and Belousova, E.A., 2004, The application of laser ablation-inductively coupled plasma-mass spectrometry to in situ U/Pb zircon geochronology: Chemical Geology, v. 211, p. 47–69, doi:10.1016/j.chemgeo.2004.06.017.

Ji, W.Q., Wu, F.Y., Chung, S.L., Li, J.X., and Liu, C.Z., 2009, Zircon U-Pb geochronology and Hf isotopic constraints on petrogenesis of the Gangdese batholith, southern Tibet: Chemical Geology, v. 262, p. 229–245, doi:10.1016/j.chemgeo.2009.01.020.

Kapp, P., Yin, A., Manning, C.E., Murphy, M., Harrison, T.M., Spurlin, M., Ding, L., Deng, X.G., and Wu, C.M., 2000, Blueschist-bearing metamorphic core complexes in the Qiangtang block reveal deep crustal structure of northern Tibet: Geology, v. 28, p. 19–22, doi:10.1130/0091-7613(2000)28<19:BMCCIT>2.0.CO;2.

Kapp, P., Yin, A., Manning, C.E., Harrison, T.M., Taylor, M.H., and Ding, L., 2003a, Tectonic evolution of the early Mesozoic blueschist-bearing Qiangtang metamorphic belt, central Tibet: Tectonics, v. 22, 1043, doi:10.1029/2002TC001383.

Kapp, P., Murphy, M.A., Yin, A., Harrison, T.M., Ding, L., and Guo, J., 2003b, Mesozoic and Cenozoic tectonic evolution of the Shiquanhe area of western Tibet: Tectonics, v. 22, 1029, doi:10.1029/2001TC001332.

Kapp, P., Yin, A., Harrison, T.M., and Ding, L., 2005, Cretaceous-Tertiary shortening, basin development, and volcanism in central Tibet: Geological Society of America Bulletin, v. 117, p. 865–878, doi:10.1130/B25595.1.

Kapp, P., DeCelles, P.G., Gehrels, G.E., Heizler, M., and Ding, L., 2007a, Geological records of the Lhasa-Qiangtang and Indo-Asian collisions in the Nima area of central Tibet: Geological Society of America Bulletin, v. 119, p. 917–933, doi:10.1130/B26033.1.

Kapp, P., DeCelles, P.G., Leier, A.L., Fabijanic, J.M., He, S., Pullen, A., and Gehrels, G.E., 2007b, The Gangdese retroarc thrust belt revealed: GSA Today, v. 17, no. 7, p. 4–9, doi:10.1130/GSAT01707A.1.

Kraus, M.J., 1999, Paleosols in clastic sedimentary rocks: Their geologic applications: Earth-Science Reviews, v. 47, p. 41–70, doi:10.1016/S0012-8252(99)00026-4.

Lee, H.Y., Chung, S.L., Wang, Y.B., Zhu, D.C., Yang, J.H., Song, B., Liu, D.Y., and Wu, F.Y., 2007, Age, petrogenesis and geological significance of the Linzizong volcanic successions in the Linzhou Basin, southern Tibet: Evidence from zircon U-Pb dates and Hf isotopes [in Chinese with English abstract]: Acta Petrolei Sinica, v. 23, p. 493–500.

Lee, H.Y., Chung, S.L., Lo, C.H., Ji, J.Q., Lee, T.Y., Qian, Q., and Zhang, Q., 2009, Eocene Neotethyan slab breakoff in southern Tibet inferred from the Linzizong volcanic record: Tectonophysics, v. 477, p. 20–35, doi:10.1016/j.tecto.2009.02.031.

Leeder, M.R., Smith, A.B., and Jixiang, Y., 1988, Sedimentology, palaeoecology and palaeoenvironmental evolution of the 1985 Lhasa to Golmud Geotraverse: Philosophical Transactions of the Royal Society of London, Series A, Mathematical and Physical Sciences, v. 327, p. 107–143, doi:10.1098/rsta.1988.0123.

Leier, A.L., DeCelles, P.G., Kapp, P., and Ding, L., 2007a, The Takena Formation of the Lhasa terrane, southern Tibet: The record of a Late Cretaceous retroarc foreland basin: Geological Society of America Bulletin, v. 119, p. 31–48, doi:10.1130/B25974.1.

Leier, A.L., DeCelles, P.G., Kapp, P., and Gehrels, G.E., 2007b, Lower Cretaceous strata in the Lhasa Terrane, Tibet, with implications for understanding the early tectonic history of the Tibetan Plateau: Journal of Sedimentary Research, v. 77, p. 809–825, doi:10.2110/jsr.2007.078.

Leier, A.L., DeCelles, P.G., Kapp, P., Gehrels, G.E., and Ding, L., 2007c, Detrital zircon geochronology of Phanerozoic sedimentary strata in the Lhasa terrane and implications for the tectonic evolution of southern Tibet: Basin Research, v. 19, p. 361–378, doi:10.1111/j.1365-2117.2007.00330.x.

Leier, A.L., McQuarrie, N., Horton, B.K., and Gehrels, G.E., 2010, Upper Oligocene conglomerates of the Altiplano, Central Andes: The record of deposition and deformation along the margin of a hinterland basin: Journal of Sedimentary Research, v. 80, p. 750–762.

Leier, A., McQuarrie, N., Garmala, C., and Eiler, J., 2013, Stable isotope evidence for multiple pulses of rapid surface uplift in the Central Andes, Bolivia: Earth and Planetary Science Letters, v. 371–372, p. 49–58, doi:10.1016/j.epsl.2013.04.025.

Li, Y.L., He, J., Wang, C.S., Santosh, M., Dai, J.G., Zhang, Y.X., Wei, Y.S., and Wang, J.G., 2013, Late Cretaceous K-rich magmatism in central Tibet: Evidence for early elevation of the Tibetan plateau?: Lithos, v. 160–161, p. 1–13, doi:10.1016/j.lithos.2012.11.019.

Liu, D.Z., Tao, X.F., Ma, R.Z., Shi, H., Zhu, L.D., and Hu, X.W., 2004, 1:250,000 geological report of Coqen County with geological map [in Chinese]: Chengdu, China, Chengdu University of Technology, p. 163–183.

Liu, Q., Jiang, W., Jian, P., Ye, P.S., Wu, Z.H., and Hu, D.G., 2006, Zircon SHRIMP U-Pb age and petrochemical and geochemical features of Mesozoic muscovite monzonitic granite at Ningzhong, Tibet [in Chinese with English abstract]: Acta Petrologica Sinica, v. 22, p. 643–652.

Liu, Z.Q.C., 1988, Geologic map of the Qinghai-Xizang Plateau and its neighboring regions: Beijing, Geologic Publishing House, scale 1:1,500,000.

Ludwig, K.R., 2001, Isoplot/Ex (rev. 2.49): A geochronological toolkit for Microsoft Excel: Berkeley Geochronology Center Special Publication 1, 58 p.

Lunt, I.A., and Bridge, J.S., 2004, Evolution and deposits of a gravelly braid bar, Sagavanirktok River, Alaska: Sedimentology, v. 51, p. 415–432, doi:10.1111/j.1365-3091.2004.00628.x.

Ma, G.L., and Yue, Y.H., 2010, Cretaceous volcanic rocks in northern Lhasa Block: Constraints on the tectonic evolution of Gangdise Arc [in Chinese with English abstract]: Acta Petrologica Et Mineralogica, v. 29, p. 525–538.

Ma, L., Wang, Q., Li, Z.X., Wyman, D.A., Jiang, Z.Q., Yang, J.H., Gou, G.N., and Guo, H.F., 2013a, The early Late Cretaceous (ca. 93 Ma) norites and hornblendites in the Milin area, eastern Gangdese: Lithosphere-asthenosphere interaction during slab roll-back and an insight into early Late Cretaceous (ca. 100–80 Ma) magmatic "flare-up" in southern Lhasa (Tibet): Lithos, v. 172–173, p. 17–30, doi:10.1016/j.lithos.2013.03.007.

Ma, L., Wang, Q., Wyman, D.A., Jiang, Z.Q., Yang, J.H., Li, Q.L., Gou, G.N., and Guo, H.F., 2013b, Late Cretaceous crustal growth in the Gangdese area, southern Tibet: Petrological and Sr-Nd-Hf-O isotopic evidence from Zhengga diorite-gabbro: Chemical Geology, v. 349–350, p. 54–70, doi:10.1016/j.chemgeo.2013.04.005.

Ma, L., Wang, Q., Wyman, D.A., Li, Z.X., Jiang, Z.Q., and Yang, J.H., 2013c, Late Cretaceous (100–89 Ma) magnesian charnockites with adakitic affinities in the Milin area, eastern Gangdese: Partial melting of subducted oceanic crust and implications for crustal growth in southern Tibet: Lithos, v. 175–176, p. 315–332, doi:10.1016/j.lithos.2013.04.006.

Mack, G.H., James, W.C., and Monger, H.C., 1993, Classification of paleosols: Geological Society of America Bulletin, v. 105, p. 129–136, doi:10.1130/0016-7606(1993)105<0129:COP>2.3.CO;2.

Meng, F.Y., Zhao, Z.D., Zhu, D.C., Zhang, L.L., Guan, Q., Liu, M., Yu, F., and Mo, X.X., 2010, Petrogenesis of Late Cretaceous adakite-like rocks in Mamba from the Eastern Gangdese, Tibet [in Chinese with English abstract]: Acta Petrologica Sinica, v. 26, p. 2180–2192.

Miall, A.D., 1978, Facies types and vertical profile models in braided river deposits: A summary, *in* Miall, A.D., ed., Fluvial Sedimentology: Canadian Society of Petroleum Geologists Memoir 5, p. 597–604.

Miall, A.D., 1996, The Geology of Fluvial Deposits: Sedimentary Facies, Basin Analysis, and Petroleum Geology: New York, Springer Publishing, 582 p.

Mo, X.X., Hou, Z.Q., Niu, Y.L., Dong, G.C., Qu, X.M., Zhao, Z.D., and Yang, Z.M., 2007, Mantle contributions to crustal thickening during continental collision: Evidence from Cenozoic igneous rocks in southern Tibet: Lithos, v. 96, p. 225–242, doi:10.1016/j.lithos.2006.10.005.

Mo, X.X., Niu, Y.L., Dong, G.C., Zhao, Z.D., Hou, Z.Q., Zhou, S., and Ke, S., 2008, Contribution of syncollisional felsic magmatism to continental crust growth: A case study of the Paleogene Linzizong volcanic succession in southern Tibet: Chemical Geology, v. 250, p. 49–67, doi:10.1016/j.chemgeo.2008.02.003.

Murphy, M.A., Yin, A., Harrison, T.M., Dürr, S.B., Chen, Z., Ryerson, F.J., Kidd, W.S.F., Wang, X., and Zhou, X., 1997, Did the Indo-Asian collision alone create the Tibetan plateau?: Geology, v. 25, p. 719–722, doi:10.1130/0091-7613(1997)025<0719:DTIACA>2.3.CO;2.

Najman, Y., Appel, E., Boudagher-Fadel, M., Bown, P., Carter, A., Garzanti, E., Godin, L., Han, J., Liebke, U., Oliver, G., Parrish, R., and Vezzoli, G., 2010, Timing of India-Asia collision: Geological, biostratigraphic, and paleomagnetic constraints: Journal of Geophysical Research, v. 115, B12416, doi:10.1029/2010JB007673.

Naylor, M.A., 1980, The origin of inverse grading in muddy debris flow deposits: A review: Journal of Sedimentary Petrology, v. 50, p. 1111–1116.

Orme, D.A., Carrapa, B., and Kapp, P., 2014, Sedimentology, provenance and geochronology of the upper Cretaceous–lower Eocene western Xigaze forearc basin, southern Tibet: Basin Research, doi:10.1111/bre.12080 (in press).

Pan, G.T., Ding, J., Yao, D.S., and Wang, L.Q., 2004, Guide book of 1:1,500,000 geologic map of the Qinghai-Xizang (Tibet) plateau and adjacent areas: Chengdu, China, Cartographic Publishing House, 148 p.

Pan, Y., 1993, Unroofing history and structural evolution of the southern Lhasa terrane, Tibetan Plateau: Implications for the continental collision between India and Asia [Ph.D. thesis]: Albany, State University of New York, 287 p.

Pullen, A., Kapp, P., Gehrels, G., DeCelles, P., Brown, E., Fabijanic, M., and Ding, L., 2008, Gangdese retroarc thrust belt and foreland basin deposits in the Damxung area, southern Tibet: Journal of Asian Earth Sciences, v. 33, p. 323–336, doi:10.1016/j.jseaes.2008.01.005.

Raymo, M.E., and Ruddiman, W.F., 1992, Tectonic forcing of late Cenozoic climate: Nature, v. 359, p. 117–122, doi:10.1038/359117a0.

Richter, F.M., Rowley, D.B., and DePaolo, D.J., 1992, Sr isotope evolution of seawater: The role of tectonics: Earth and Planetary Science Letters, v. 109, p. 11–23, doi:10.1016/0012-821X(92)90070-C.

Rohrmann, A., Kapp, P., Carrapa, B., Reiners, P.W., Guynn, J., Ding, L., and Heizler, M., 2012, Thermochronologic evidence for plateau formation in central Tibet by 45 Ma: Geology, v. 40, p. 187–190, doi:10.1130/G32530.1.

Rowley, D., and Currie, B., 2006, Paleo-altimetry of the late Eocene to Miocene Lunpola basin, central Tibet: Nature, v. 439, p. 677–681, doi:10.1038/nature04506.

Scherer, E., Munker, C., and Mezger, K., 2001, Calibration of the lutetium-hafnium clock: Science, v. 293, p. 683–687, doi:10.1126/science.1061372.

Scott, R., Wan, X., Sha, J., and Wen, S., 2010, Rudists of Tibet and the Tarim basin, China: Significance to Requieniidae phylogeny: Journal of Paleontology, v. 84, p. 444–465, doi:10.1666/09-137.1.

Searle, M.P., Windley, B.F., Coward, M.P., Cooper, D.J.W., Rex, A.J., Rex, D.C., Li, T.D., Xiao, X.C., Jan, Q., Thakur, V., and Kumar, S., 1987, The closing of Tethys and the tectonics of the Himalaya: Geological Society of America Bulletin, v. 98, p. 678–701, doi:10.1130/0016-7606(1987)98<678:TCOTAT>2.0.CO;2.

Staisch, L.M., Niemi, N.A., Hong, C., Clark, M.K., Rowley, D.B., and Currie, B., 2014, A Cretaceous-Eocene depositional age for the Fenghuoshan Group, Hoh Xil Basin: Implications for the tectonic evolution of the northern Tibet Plateau: Tectonics, v. 33, p. 281–301, doi:10.1002/2013TC003367.

Tapponnier, P., Zhiqin, X., Roger, F., Meyer, B., Arnaud, N., Wittlinger, G., and Jingsui, Y., 2001, Oblique stepwise rise and growth of the Tibet Plateau: Science, v. 294, p. 1671–1677, doi:10.1126/science.105978.

Van Achterbergh, E., Ryan, C.G., Jackson, S.E., and Griffin, W.L., 2001, Data reduction software for LA-ICPMS: Appendix, *in* Sylvester, P., ed., Laser-Ablation-ICPMS in the Earth Sciences: Principles and Applications: Mineralogical Association of Canada Short Course 29, p. 239–243.

Volkmer, J.E., Kapp, P., Guynn, J.H., and Lai, Q., 2007, Cretaceous-Tertiary structural evolution of the north central Lhasa terrane, Tibet: Tectonics, v. 26, TC6007, doi:10.1029/2005TC001832.

Wang, B.D., Xu, J.F., Liu, B.M., Chen, J.L., Wang, L.Q., Guo, L., Wang, D.B., and Zhang, W.P., 2013, Geochronology and ore-forming geological background of ~90 Ma porphyry copper deposit in the Lhasa Terrane, Tibet Plateau [in Chinese with English abstract]: Acta Geologica Sinica, v. 87, p. 71–80.

Wang, C., and Liu, Z., 1999, Xigaze forearc basin and Yarlung Zangbo suture zone, Tibet [in Chinese]: Beijing, Geological Publishing House, 237 p.

Wang, C., Zhao, X., Liu, Z., Lippert, P.C., Graham, S.A., Coe, R.S., Yi, H., Zhu, L., Liu, S., and Li, Y., 2008, Constraints on the early uplift history of the Tibetan Plateau: Proceedings of the National Academy of Sciences of the United States of America, v. 105, p. 4987–4992, doi:10.1073/pnas.0703595105.

Wang, C., Li, X., Liu, Z., Li, Y., Jansa, L., Dai, J., and Wei, Y., 2012, Revision of the Cretaceous–Paleogene stratigraphic framework, facies architecture and provenance of the Xigaze forearc basin along the Yarlung Zangbo suture zone: Gondwana Research, v. 22, p. 415–433, doi:10.1016/j.gr.2011.09.014.

Wang, C., Dai, J., Zhao, X., Li, Y., Graham, S., He, D., Ran, B., and Meng, J., 2014a, Outward-growth of the Tibetan Plateau during the Cenozoic: A review: Tectonophysics, v. 621, p. 1–43, doi:10.1016/j.tecto.2014.01.036.

Wang, J.G., Hu, X.M., Jansa, L., and Huang, Z.C., 2011, Provenance of the Upper Cretaceous–Eocene deep-water sandstones in Sangdanlin, southern Tibet: Constraints on the timing of initial India-Asia collision: The Journal of Geology, v. 119, p. 293–309, doi:10.1086/659145.

Wang, Q., Zhu, D.C., Zhao, Z.D., Liu, S.A., Chung, S.L., Li, S.M., Liu, D., Dai, J.G., Wang, L.Q., and Mo, X.X., 2014b, Origin of the ca. 90 Ma magnesia-rich volcanic rocks in SW Nyima, central Tibet: Products of lithospheric delamination beneath the Lhasa-Qiangtang collision zone: Lithos, v. 198–199, p. 24–37, doi:10.1016/j.lithos.2014.03.019.

Wen, D.R., Liu, D.Y., Chung, S.L., Chu, M.F., Ji, J.Q., Zhang, Q., Song, B., Lee, T.Y., Yeh, M.W., and Lo, C.H., 2008, Zircon SHRIMP U-Pb ages of the Gangdese Batholith and implications for Neotethyan subduction in southern Tibet: Chemical Geology, v. 252, p. 191–201, doi:10.1016/j.chemgeo.2008.03.003.

Wu, F., Ji, W., Liu, C., and Chung, S., 2010, Detrital zircon U-Pb and Hf isotopic data from the Xigaze forearc basin: Constraints on Transhimalayan magmatic evolution in southern Tibet: Chemical Geology, v. 271, p. 13–25, doi:10.1016/j.chemgeo.2009.12.007.

Wu, F.Y., Ji, W.Q., Wang, J.G., Liu, C.Z., Chung, S.L., and Clift, P.D., 2014, Zircon U-Pb and Hf isotopic constraints on the onset time of India-Asia collision: American Journal of Science, v. 314, p. 548–579, doi:10.2475/02.2014.04.

Xu, Q., Ding, L., Zhang, L.Y., Cai, F.L., Lai, Q.Z., Yang, D., and Zeng, J.L., 2013, Paleogene high elevations in the Qiangtang Terrane, central Tibetan Plateau: Earth and Planetary Science Letters, v. 362, p. 31–42, doi:10.1016/j.epsl.2012.11.058.

XZBGM (Xizang Bureau of Geology and Mineral Resources), 1993, Regional geology of Xizang Autonomous Region, China, with geologic map: Beijing, Geological Publishing House, 707 p., scale 1:1,500,000.

Yao, X.F., Tang, J.X., Li, Z.J., Deng, S.L., Ding, S., Hu, Z.H., and Zhang, Z., 2013, The redefinition of the ore-forming porphyry's age in Gaerqiong skarn-type gold-copper deposit, Western Bangong Lake–Nujiang River metallogenic belt, Xizang(Tibet) [in Chinese with English abstract]: Geological Review, v. 59, p. 193–201.

Yin, A., and Harrison, T.M., 2000, Geologic evolution of the Himalayan-Tibetan orogen: Annual Review of Earth and Planetary Sciences, v. 28, p. 211–280, doi:10.1146/annurev.earth.28.1.211.

Yin, J., Xu, J., Liu, C., and Li, H., 1988, The Tibetan Plateau: Regional stratigraphic context and previous work: Philosophical Transactions of the Royal Society of London, Series A, Mathematical and Physical Sciences, v. 327, p. 5–52, doi:10.1098/rsta.1988.0121.

Yu, H.X., Chen, J.L., Xu, J.F., Wang, B.D., Wu, J.B., and Liang, Y.H., 2011, Geochemistry and origin of Late Cretaceous (~90 Ma) mineral porphyry of Balazha in mid-northern Lhasa terrane, Tibet [in Chinese with English abstract]: Acta Petrolei Sinica, v. 27, p. 2011–2022.

Zhang, H.F., Xu, W.C., Guo, J.Q., Zong, K.Q., Cai, H.M., and Yuan, H.L., 2007a, Zircon U-Pb and Hf isotopic composition of deformed granite in the southern margin of the Gangdese belt, Tibet: Evidence for early Jurassic subduction of Neo-Tethyan oceanic slab [in Chinese with English abstract]: Acta Petrolei Sinica, v. 23, p. 1347–1353.

Zhang, H.F., Xu, W.C., Guo, J.Q., Zong, K.Q., Cai, H.M., and Yuan, H.L., 2007b, Indosinian orogenesis of the Gangdese terrane: Evidences from zircon U-Pb dating and petrogenesis of granitoids: Earth Science, v. 32, p. 155–166.

Zhang, K.J., 2000, Cretaceous paleogeography of Tibet and adjacent areas (China): Tectonic implications: Cretaceous Research, v. 21, p. 23–33, doi:10.1006/cres.2000.0199.

Zhang, K.J., Xia, B.D., Wang, G.M., Li, Y.T., and Ye, H.F., 2004, Early Cretaceous stratigraphy, depositional environments, sandstone provenance, and tectonic setting of central Tibet, western China: Geological Society of America Bulletin, v. 116, p. 1202–1222, doi:10.1130/B25388.1.

Zhang, K.J., Zhang, Y., Tang, X., and Xia, B., 2012, Late Mesozoic tectonic evolution and growth of the Tibetan plateau prior to the Indo-Asian collision: Earth-Science Reviews, v. 114, p. 236–249, doi:10.1016/j.earscirev.2012.06.001.

Zhang, Q., Ding, L., Cai, F., Xu, X., Zhang, L., Xu, Q., and Willems, H., 2011, Early Cretaceous Gangdese retro-arc foreland basin evolution in the Selin Co basin, central Tibet: Evidence from sedimentology and detrital zircon geochronology, *in* Gloaguen, R., and Ratschbacher, L., eds., Growth and Collapse of the Tibetan Plateau: Geological Society of London Special Publication 353, p. 27–44, doi:10.1144/SP353.3.

Zhou, C.Y., Zhu, D.C., Zhao, Z.D., Xu, J.F., Wang, L.Q., Chen, H.H., Xie, L.W., Dong, G.C., and Zhou, S., 2008, Petrogenesis of Daxiong pluton in western Gangdese, Tibet: Zircon U-Pb dating and Hf isotopic constraints [in Chinese with English abstract]: Acta Petrolei Sinica, v. 24, p. 348–358.

Zhu, D.C., Pan, G.T., Mo, X.X., Wang, L.Q., Liao, Z.L., Zhao, Z.D., Dong, G.C., and Zhou, C.Y., 2006, Late Jurassic–Early Cretaceous geodynamic setting in middle-northern Gangdese: New insights from volcanic rocks [in Chinese with English abstract]: Acta Petrolei Sinica, v. 22, p. 534–546.

Zhu, D.C., Mo, X.X., Zhao, Z.D., Xu, J.F., Zhou, C.Y., Sun, C.G., Wang, L.Q., Chen, H.H., Dong, G.C., and Zhou, S., 2008, Zircon U-Pb geochronology of Zenong Group volcanic rocks in Coqen area of Gangdese, Tibet and tectonic significance [in Chinese with English abstract]: Acta Petrolei Sinica, v. 24, p. 401–412.

Zhu, D.C., Mo, X.X., Niu, Y.L., Zhao, Z.D., Wang, L.Q., Liu, Y.S., and Wu, F.Y., 2009, Geochemical investigation of Early Cretaceous igneous rocks along an east-west traverse throughout the central Lhasa Terrane, Tibet: Chemical Geology, v. 268, p. 298–312, doi:10.1016/j.chemgeo.2009.09.008.

Zhu, D.C., Zhao, Z.D., Niu, Y.L., Mo, X.X., Chung, S.L., Hou, Z.Q., Wang, L.Q., and Wu, F.Y., 2011a, The Lhasa Terrane: Record of a microcontinent and its histories of drift and growth: Earth and Planetary Science Letters, v. 301, p. 241–255, doi:10.1016/j.epsl.2010.11.005.

Zhu, D.C., Zhao, Z.D., Niu, Y.L., Dilek, Y., and Mo, X.X., 2011b, Lhasa terrane in southern Tibet came from Australia: Geology, v. 39, p. 727–730, doi:10.1130/G31895.1.

Science Editor: Christian Koeberl
Associate Editor: Zheng-Xiang Li

Manuscript Received 22 May 2014
Revised Manuscript Received 9 December 2014
Manuscript Accepted 15 January 2015

Printed in the USA